

ULRR

Review—Use of impedance spectroscopy for the estimation of Li-ion battery state of charge, state of health and internal temperature

Item Type	Article
Authors	McCarthy, Kieran;Gullapalli, Hemtej;Ryan, Kevin M.;Kennedy, Tadhg
Citation	Journal of The Electrochemical Society;168 (8) 080517
Publisher	Electrochemical Society
Download date	2026-06-08 17:55:44
Item License	https://creativecommons.org/licenses/by-nc-sa/1.0/
Link to Item	https://hdl.handle.net/10344/10501

ACCEPTED MANUSCRIPT

Review—Use of Impedance Spectroscopy for the Estimation of Li-ion Battery State of Charge, State of Health and Internal Temperature

To cite this article before publication: Tadhg Kennedy *et al* 2021 *J. Electrochem. Soc.* in press <https://doi.org/10.1149/1945-7111/ac1a85>

Manuscript version: Accepted Manuscript

Accepted Manuscript is “the version of the article accepted for publication including all changes made as a result of the peer review process, and which may also include the addition to the article by IOP Publishing of a header, an article ID, a cover sheet and/or an ‘Accepted Manuscript’ watermark, but excluding any other editing, typesetting or other changes made by IOP Publishing and/or its licensors”

This Accepted Manuscript is © 2021 The Author(s). Published by IOP Publishing Ltd..

This article can be copied and redistributed on non commercial subject and institutional repositories.

Although reasonable endeavours have been taken to obtain all necessary permissions from third parties to include their copyrighted content within this article, their full citation and copyright line may not be present in this Accepted Manuscript version. Before using any content from this article, please refer to the Version of Record on IOPscience once published for full citation and copyright details, as permissions will likely be required. All third party content is fully copyright protected, unless specifically stated otherwise in the figure caption in the Version of Record.

View the [article online](#) for updates and enhancements.

**Review—Use of Impedance Spectroscopy for the Estimation
of Li-ion Battery State of Charge, State of Health and
Internal Temperature**

Journal:	<i>Journal of The Electrochemical Society</i>
Manuscript ID	JES-104321.R1
Manuscript Type:	Review Paper
Date Submitted by the Author:	25-Jun-2021
Complete List of Authors:	Kennedy, Tadhg; University of Limerick, Chemical Sciences Gullapalli, Hemtej; Analog Devices International Ryan, Kevin; University of Limerick, Materials and Surface Science Institute and Department of Chemical and Environmental Sciences Mccarthy, Kieran; University of Limerick, Chemical Sciences
Keywords:	Electrochemical impedance spectroscopy, Batteries – Li-ion, State of charge, State of health, Internal temperature

SCHOLARONE™
Manuscripts

Review—Use of Impedance Spectroscopy for the Estimation of Li-Ion Battery State of Charge, State of Health and Internal Temperature

Kieran Mc Carthy,¹ Hemtej Gullapalli,² Kevin M. Ryan,^{1,*z} and Tadhg Kennedy^{1,z}

¹Bernal Institute and Department of Chemical Sciences, University of Limerick, V94 T9PX Limerick, Ireland

²Analog Devices, Boston, Massachusetts 02110, United States

*Electrochemical Society Member.

^zE-mail: Tadhg.kennedy@ul.ie & Kevin.M.Ryan@ul.ie

Abstract

The rapid adoption of electric vehicles (EVs) and the evolving needs of portable electronic devices has intensified the need for enhanced state diagnosis of Li-ion batteries (LIBs). As the applications for LIBs continue to grow, so too does their operational requirements; ranging from faster charging and improved safety to optimized energy control and extended lifespan. In order to keep pace with the growing requirements of LIBs, improvements in the monitoring of battery states must be achieved. Although electrochemical impedance spectroscopy (EIS) has existed since the 1960's, its potential as a diagnosis tool has only received widespread attention in recent years. In this paper, a detailed review on the applicability of impedance measurements for the estimation of the vital battery parameters of state of charge (SOC), state of health (SOH) and internal temperature (IT) has been performed.

1. Introduction

The management of Li-ion batteries (LIBs) is of the utmost importance for the safety, efficiency and expected lifespan of these energy storage systems.[1] The ability to accurately estimate vital battery states is a key requirement for advanced battery monitoring. Credible estimates of state of charge (SOC), state of health (SOH) and internal temperature (IT) are

1
2
3 essential for efficient charging, health monitoring and thermal management of LIBs. Due to
4 their long lifespan and high energy density, LIBs are now the most widely used energy storage
5 technology for portable electronic devices.[2, 3] However, clear challenges remain in the
6 controlling and monitoring of the important battery states of SOC, SOH and IT. Consequences
7 of poor battery management include rapid degradation of cell performance, decreased
8 lifespan and possibly even a fire or explosive event. As such, the importance of operating a
9 LIB within its safe operating window is paramount, which is characterised by a battery's
10 voltage, temperature and current.[2] Furthermore, the increasing adoption of EVs and
11 integration of batteries into the electricity grid for stationary energy storage will require an
12 improved monitoring capability to prolong their useable lifespan as well as ensuring their safe
13 and optimal operation.[4] A key factor in recognising when a battery starts to degrade or
14 operate inefficiently is the battery management system (BMS), which continuously monitors
15 the battery's current state.

16
17 Although LIBs have seen advancements in battery technology, issues regarding their
18 monitoring and regulation remain. Unfortunately, BMS developments have not advanced at
19 the same pace seen with the enormous improvements of Li-ion technology, hindered by
20 difficulties regarding battery modelling, battery state estimation and cell balancing.[5] Owing
21 to the complicated electrochemical nature of LIBs, sensing of only voltage, current and
22 surface temperature cannot result in highly accurate estimates of SOC, SOH or IT. LIBs are
23 highly susceptible to internal and external operating conditions such as changes in
24 temperature, charging / discharging current and voltage window and so special attention
25 must be paid to LIBs and the BMS to ensure they achieve a long operating life.

26
27 Research in the implementation of impedance-based state estimation has been
28 ongoing for many years with much research aiming to establish a relationship between
29 impedance and the SOC, SOH and IT. [6-12] EIS is a well-understood battery characterisation
30 method that has been used for several decades in the monitoring and understanding of
31 internal electrochemical processes, with tests on batteries dating back to 1963.[13]
32 Advantages of EIS include its non-destructive nature, the insight it provides into internal
33 degradation processes and its tolerance to integrator drift, thus, it has widely been applied
34 for characterising and modelling the behaviour of batteries.[14-18] EIS can be used to develop
35 dynamic battery models whose parameters correlate to the electrochemical processes that

1
2
3 occur within a battery e.g. charge-transfer resistance, diffusion etc.[19] Existing studies have
4 demonstrated an intrinsic relationship between battery impedance and SOH, SOC and IT.[10-
5 12, 20-32] Many studies have used different frequency ranges and EIS elements to estimate
6 the battery states, with no overall consensus existing on which frequencies or elements give
7 the best estimates. The majority of studies have been laboratory based and performed on
8 small capacity LIBs with few field experiments.[8, 33] To date, the practical implementation
9 of an impedance capable device on portable electronics has been limited by the cost, power
10 inefficiency and complicated nature of the equipment. However, recent advancements in
11 electronic technology has made chip-scale impedance sensing a viability, igniting a newfound
12 interest in impedance for battery monitoring.[8, 33-37]

21
22 This paper intends to provide a wide-ranging review of the existing literature on the
23 use of impedance for the estimation of SOC, SOH and IT. In-depth analysis of the estimation
24 model, part of impedance utilised, battery chemistry and accuracy of each model has been
25 performed. At time of writing, no other review exists that discusses impedance based
26 battery state estimation for SOC, SOH and IT to this degree in one paper. A considerable
27 number of studies exist for each, with the exception of fault detection, which has not until
28 recently received adequate attention. It must be noted that this review only addresses
29 published data regarding EIS for secondary or rechargeable LIB state estimation. The first
30 part of this paper discusses the design and role of the BMS in battery-powered systems, the
31 principle behind the functioning of EIS and how useful information can be extracted from
32 the impedance spectra of LIBs. Next, the practical implementation of an EIS capable device
33 in real-world applications is explored with focus on cost, power consumption and
34 measurement quality. This is followed by an investigation into the use of equivalent circuit
35 models (ECMs) and specific single or multiple frequency's that show high sensitivity to
36 particular battery states. The final part of this review focuses on an in-depth analysis of the
37 application of EIS for estimation of SOC, SOH and IT. Current approaches used for SOH, SOC
38 and IT battery estimation are also explored. The volume of published literature in reputable
39 journals in recent years regarding EIS gives strength to the notion that it is a valuable tool
40 for estimating the states of a battery (Fig. 1). In the last 10 years there has been a three-fold
41 increase in total publications for EIS based state estimation. This breaks down to an increase
42 of 13.5x for temperature, 4.8x for SOH and 2.2x for SOC.

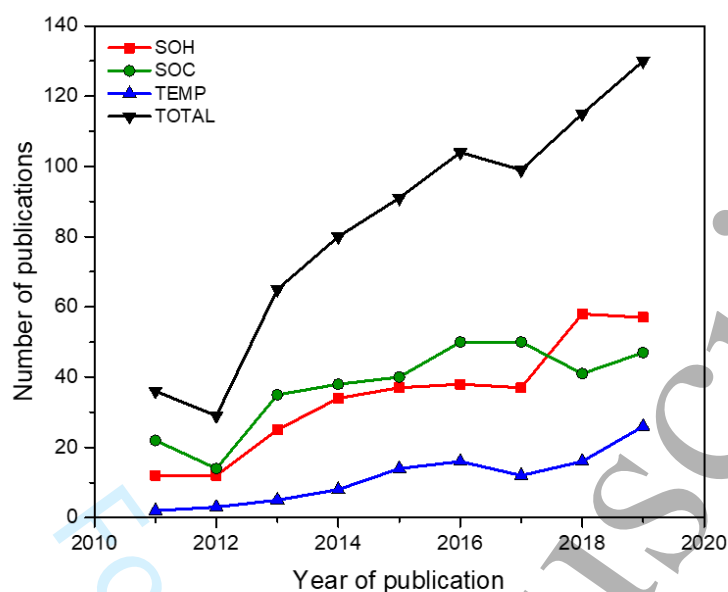


Fig. 1. Number of publications by year that use impedance in the calculation of battery SOH, SOC and IT determined via Web of Science using search words 'Impedance', 'Battery' and 'SOH / SOC / Temperature'.

2. Battery Management System

LIBs require the use of a BMS to monitor their current state, guarantee they are cycled within strict safety limits and ensure the optimal use of their available capacity.[38, 39]. This is particularly true for the large battery packs in EVs, which is generally comprised of hundreds of cells in various series-parallel connections in order to meet the voltage requirements of the vehicle.[40] Special attention is required to ensure each battery is effectively managed and controlled by the BMS. This makes the BMS requirements in an EV much more complicated than those for portable electronic devices, which typically contain a single cell. Continual characterization of the batteries present state ensures the maximum extension of battery life as well as ensuring it is operated within safe cycling limits.[5, 38, 39] SOH, SOC and IT are the most important states that a BMS calculates but a BMS also controls battery identification and cell balancing.[20, 41-47] Based on these requirements, the BMS has evolved from a rudimentary monitoring unit to an intelligent device that monitors, calculates and determines what the battery should do given its current state. An effective battery model is a prerequisite for effective battery state monitoring, thermal management, fault detection and

1
2
3 charge/discharge control.[48] As the internal battery states of SOC, SOH and IT cannot be
4 measured directly, accurate estimation methods need to be used. The charge and discharge
5 procedure of a battery is particularly important to the BMS due to the impact it can have on
6 the operational safety and system requirements of a LIB. A BMS must employ an intelligent
7 charging and discharging strategy that will protect the battery against damage, limit large
8 changes in temperature and ensure optimal energy usage.[49] This is particularly important
9 for EVs where fast charging is the norm. A slow charge will extend the time the EV is
10 unavailable for usage, whereas a fast charge may adversely affect the current condition of the
11 battery causing premature ageing. Charging and discharging procedures also vary depending
12 on the current battery temperature. In comparison to other battery chemistries, Li-ion
13 batteries have stable long-term performance but are more susceptible to damage when
14 operated at high or low temperatures. Incorrect operation at extreme high or low
15 temperatures will increase the rate of degradation in the battery dramatically.[50, 51]
16 Traditionally, battery states have been calculated by monitoring the voltage, current and
17 surface temperature (VIT) of the battery using onboard sensors and then applying a model
18 for estimation.[2] The battery model utilises measurements from each variable to achieve an
19 estimate of its current state. Once the thermal and electric behaviour of the battery has been
20 captured, the charging and discharging procedures can be optimised using a specially
21 designed algorithm. If an abnormal situation is detected during operation, the alarm module
22 of the BMS will work to eliminate this issue. In many applications, due to the inaccuracy
23 associated with battery state estimation, overdesigning the battery pack with an increased
24 capacity is often done in order to ensure the rated capacity lies within the SOC margin of error
25 and to place conservative limits on operational temperature and battery health.[34, 52] For
26 example, a 2.8 Ah rated Li-ion battery may be able to safely store 3 Ah worth of charge
27 however, due to the inaccuracy associated with SOC estimation (typically 5 %) the battery's
28 total capacity is limited to 2.8 Ah to ensure the battery never overcharges or over-discharges.
29
30
31
32
33
34
35
36
37
38
39
40
41
42
43
44
45
46
47
48
49
50

51 A BMS is a computer system that uses sensors, actuators and analytical models to
52 perform tasks such as monitoring charging and discharging cycles, communication, storing
53 data, cell balancing, thermal management, estimating the systems SOC and SOH and
54 measuring the voltage, current and temperature.[49] The real-time collection of data is used
55 to ensure system is operated safely and determine the current state of the battery. The
56
57
58
59
60

1
2
3 battery state is then used to determine the charging and discharging procedure among the
4 cells and is further sent to the user via the interface. If any of these parameters exceed their
5 limits, the BMS generates an alarm or stops the current flow in or out of the battery. The BMS
6 is only a small fraction of the overall cost of the battery but guarantees its lifetime. Three of
7 the major monitoring issues of existing BMSs have been SOC estimation, SOH estimation and
8 thermal regulation. Overall, an effective BMS should include and perform these
9 operations:[5]

- 16 • Communication with batteries
- 17 • Safety protection and fault detection
- 18 • Control the charge and discharge procedure
- 19 • Capacity balancing of cells
- 20 • Thermal management
- 21 • Predict the current state of the battery

22
23
24
25
26
27
28
29
30
31 A BMS architecture can be split into two fundamental sections which are discussed below
32 (Fig. 2):

33
34
35 *Hardware:* The hardware includes sensors that monitor the voltage, current and surface
36 temperature of the battery. A surface thermocouple or thermistor are commonly used for
37 temperature estimation. All these measurements must be acquired simultaneously to ensure
38 a reliable updating of battery models. The timestamp of each measurement must be identical
39 to ensure all data is synced. Additionally, a high sampling rate is required to guarantee the
40 fast-changing kinetics of the battery system can be monitored.[53] Recent advancements in
41 wireless communications has increased the volume of data that can be communicated
42 between the charger and battery. EIS has been proposed as a potential new addition to the
43 hardware architecture to monitor cell impedance.

44
45
46
47
48
49
50
51
52
53 *Software:* The software of a BMS can be thought of as the 'brain' of the system as it monitors
54 all data acquired from the hardware, controls internal communication between different
55 hardware blocks, manages battery protection and estimates important battery state
56 parameters such as SOC, SOH and temperature.[44] In a battery pack, the software is also
57 responsible for cell balancing and updating all battery functions. Cell balancing ensures the
58
59
60

SOC value of all batteries are as close as possible to prevent any overcharging or over-discharging. The user of the battery-powered device will receive information about the current state of the battery via a user interface.

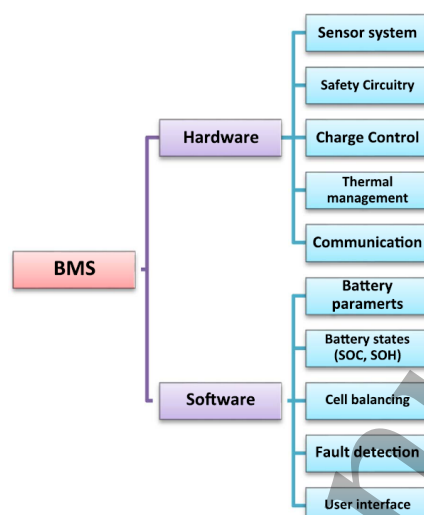


Fig. 2. Diagram showing the parameters controlled by the hardware and software sections in a BMS.[44]¹

3. Electrochemical Impedance Spectroscopy

EIS is used to characterise the changing behaviour of a battery in response to an injected signal of a small amplitude.[54-56] In theory, any excitation signal can be used however, in practice, a sine wave is the most common.[57] Impedance is obtained by applying a superimposed sinusoidal excitation, at a specific frequency f , and measuring the response from the battery, which is based on the battery impedance. The excitation signal can be current or voltage based although the potentiostatic approach is less common in battery applications.[17] In galvanostatic mode, a sinusoidal current is superimposed on the battery's d.c. current (I) yielding the following equation:[20]

¹ Reprinted from Energies, Vol. 4 /11, Yinjiao Xing, Eden W. M. Ma, Kwok L. Tsui & Michael Pecht, Battery Management Systems in Electric and Hybrid Vehicles/Electric and Hybrid Vehicles, 1840-1857, Copyright (2011), with permission from MDPI.

$$\Delta I = I_{max} \sin(2\pi ft) \quad (1)$$

The voltage response from the excitation signal can then be measured:

$$\Delta V = V_{max} \sin(2\pi ft + \phi) \quad (2)$$

where the amplitude of the voltage response V_{max} and the phase ϕ are determined by the particular frequency. In potentiostatic mode, the opposite occurs where a sinusoidal voltage is superimposed on the battery's d.c. voltage (V):[20] Likewise, the amplitude of the current response I_{max} and the phase ϕ are determined by the frequency. The impedance for both galvanostatic and potentiostatic methods is defined by:[20]

$$Z(f) = \frac{V_{max}}{I_{max}} e^{j\phi} \quad (3)$$

EIS gives an accurate impedance measurement over a wide band of frequencies, thus providing an in-depth characterisation method for the analysis of battery behaviour. The electrochemical impedance is given as a complex number, comprised of real and imaginary parts.[20] EIS is usually performed while the cell is in open-circuit and not during charging or discharging. The impedance is dependent on the frequency used, the magnitude of perturbation from the voltage and current and the phase shift between waves as well as other parameters such as battery SOC, SOH and IT [58]. Impedance measurements must be performed under pseudo-linear conditions. To ensure this, the voltage amplitude must not exceed approximately 10 mV.[59] Under pseudo-linear conditions, Ohms law can be applied. In a pseudo-linear system, a sinusoidal perturbation input produces a sinusoidal output at the exact same frequency, but the phase and amplitude are shifted [20, 60]. This condition can easily be achieved in potentiostatic mode where a voltage amplitude can be set by the equipment.[20] In galvanostatic mode, the current amplitude must be set so the resultant voltage response is or is close to 10 mV.

4. Impedance Spectra

An impedance spectrum is formed as the different perturbation frequencies give different responses. Impedance spectra can be viewed in a Bode plot or more commonly in a Nyquist plot. The horizontal x-axis of a Nyquist plot represents the real impedance, denoted by Z' , while the vertical y-axis represents the imaginary impedance and is denoted by Z'' . [61] Frequency is not given but it is assumed to be highest on the left and decreases as the plot moves to the right. A Nyquist plot is frequently used in battery research due to the useful information that can be obtained [62]. The characteristic shape of a Nyquist plot is presented in Fig. 3a with five distinct sections, each relating to a particular kinetic process. [63]

1. *Induction*: At high frequencies, induction is caused by metallic parts present in the battery and the wires used to perform the AC measurement. [63] Inductance is observed in the kilohertz range and only contains an imaginary impedance. Inductance is also caused by the porosity of the electrodes and the physical inductance of the test wires (44).
2. *Ohmic resistance*: Ohmic resistance (R_o) is represented by the intersection of the spectra with the real or x-axis. It is the total resistance of the electrolyte, active material, current collector and separator. As a resistor does not have a phase dependency, there will be no imaginary impedance and it will appear as a single point on the x-axis. It is predominantly composed of the resistance of the electrolyte but is also affected by the electrode metals, electrode leads, terminals and the resistance between contact points [64]. Decomposition of the electrolyte has a significant impact on the impedance of a battery. Loss of electrolyte happens over time due to reactions with the electrodes. This loss increases electrolyte resistance by the reduction of Li-ion mobility. As such, an increase in R_o is accompanied by a decrease in conductivity.
3. *Semi-circle (high frequency)*: This semicircle shape is related to the solid electrolyte interface (SEI) that forms on the surface of the anode during cycling through the decomposition of the electrolyte at high voltages. The product of this reaction forms a layer of organic and inorganic substances on the surface of the electrode. [65] This layer contains lithium, therefore SEI growth results in the loss of cyclable lithium, reducing the cell capacity. The SEI prevents the electrolyte coming into direct contact with the active material so once the SEI layer has formed, electrolyte is prevented

1
2
3 from reaching the electrode surface, suppressing further growth. An additional effect
4 of SEI formation is the increase of cell internal resistance, as the SEI layer impedes
5 lithium intercalation.
6
7

- 8
9 4. *Semi-circle (low frequency)*: The low frequency semicircle characterizes the double
10 layer capacitance (C_{dl}) and charge-transfer resistances (R_{ct}) present at the interface
11 between the battery electrodes and electrolyte. The double layer effect occurs at this
12 interface as ions adsorb onto the surface of the electrode. [66]. It is composed of two
13 parallel layers of opposite charges encompassing the electrode. When voltage is
14 applied to the electrode, two layers of polarized ions are formed. The first layer
15 originates from the surface of the electrode. The second layer has an opposite polarity
16 and originates from the electrolyte. These layers are separated by a single layer of
17 solvent molecules. This solvent layer behaves like a dielectric in a capacitor.[67] As
18 such, it is modelled as a capacitor. Charge transfer resistance involves the movement
19 of electrons from one phase to another i.e. electrode (solid) to the electrolyte (liquid).
20 When direct current is transferred across the electrode – electrolyte interface, some
21 resistance is encountered. This transfer of electrons occurs at a certain speed and is
22 dependent on temperature, potential and concentration of reactants. A charge
23 boundary of opposing polarity is formed at the electrode surface and electrolyte.
24 These processes are described by a parallel connection of a resistor with a capacitor
25 or a constant phase element (CPE).
26
27
28
29
30
31
32
33
34
35
36
37
38
39
40 5. *Diffusion*: Warburg diffusion characterizes the diffusion processes within the battery
41 and appears as a straight line usually at an approximate 45° angle.[68] There is no
42 common circuit element that can model Warburg impedance. As such, a CPE denoted
43 'W' is used. Warburg impedance is represented by a diagonal line that has a slope of
44 approximately 45° on a Nyquist plot. On a Bode plot, a phase shift of 0.5 can be
45 observed.
46
47
48
49
50
51
52
53
54
55
56
57
58
59
60

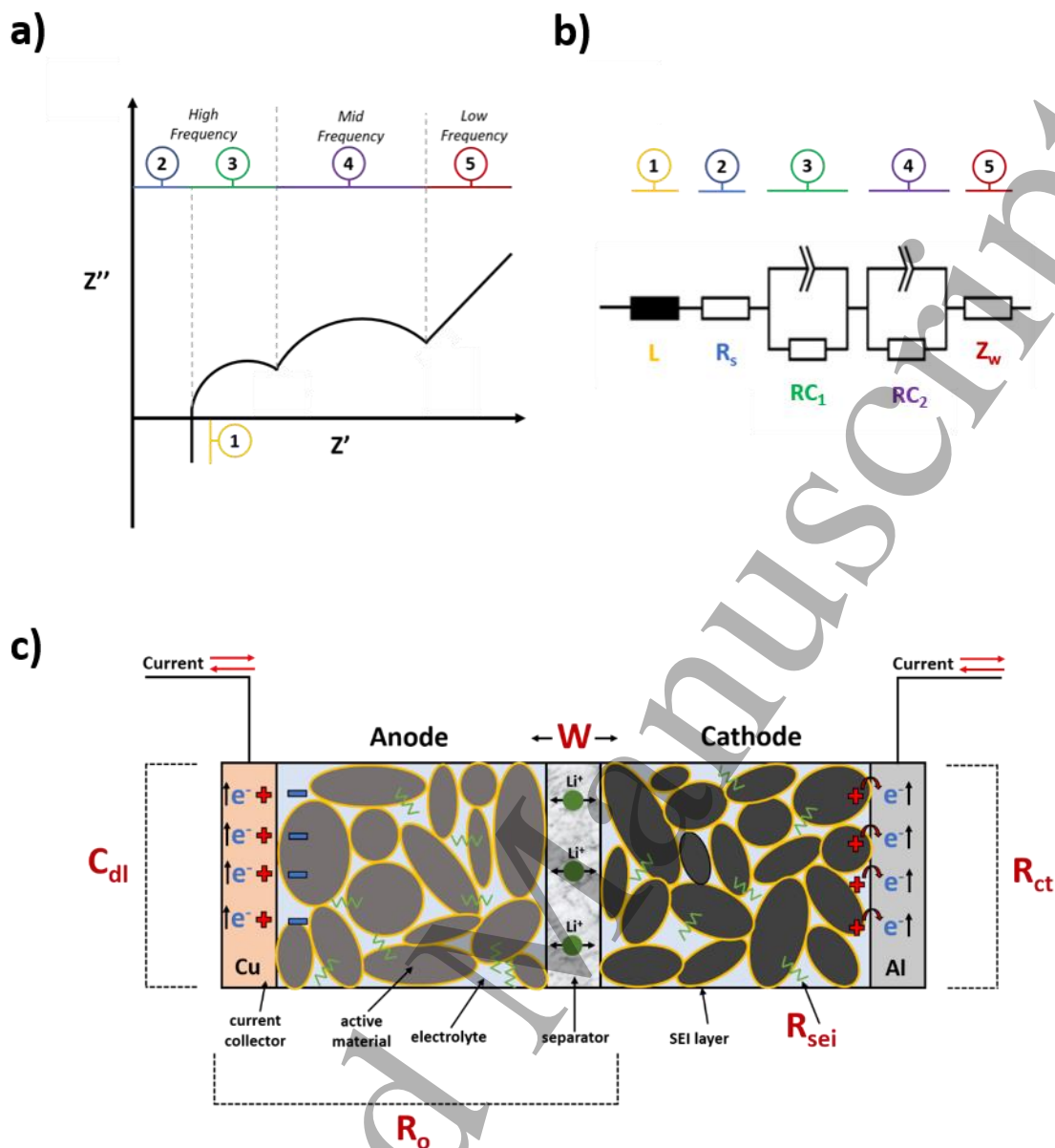


Fig. 3. Schematic showing a) the impedance response of a typical LIB in a Nyquist plot, b) the accompanying equivalent circuit model and c) Sectional diagram of a Li-ion battery with physical phenomena.

The EIS spectra of a LIB consists of three parts: high-frequency, mid-frequency and low frequency regions. It must be noted that it is often not possible to differentiate the high and low frequency semicircles from one another. Positive imaginary impedances correspond to the inductive nature of the cell interconnections. Negative imaginary impedances relate to a number of factors such as the capacitive phenomena that the electrolyte / electrodes

1
2
3 interface and charge transfer resistances.[26] Data is usually interpreted through the
4 modelling and fitting of the impedance data with an ECM. Each component in an ECM mimics
5 an electrochemical process occurring inside the battery (Fig. 3b).[69] ECMs use resistors and
6 capacitors to model the behaviour of batteries during charge and discharge.[60] They are
7 widely used due to the simplicity in which they can be implemented, the low number of
8 parameters required and the computational ease in which they operate. [61, 62] ECMs can
9 be divided into first order, second order and third order models, depending on the number
10 of RC networks.[63] For example, a first order model contains only one RC network, a second
11 order model two parallel RC networks and a third order model three parallel RC networks.
12 The number of RC networks can be increased to enhance accuracy at the expense of time and
13 computational power.[59, 64, 65] The most basic ECM, known as a Randle or Thevenin model,
14 consists of only one RC network. A second parallel RC network can be added to mimic battery
15 concentration and polarization effects.[25] The values for the resistors and capacitors are
16 determined using calculated test data. In addition, any of the aforementioned models can be
17 fitted with a hysteresis state to model for battery hysteresis during charging and discharging
18 [59].

19
20
21
22
23
24
25
26
27
28
29
30
31
32
33 Fig. 3c illustrates a sectional representation of a LIB and the related physical phenomena.
34 The diagram shows how the components of an ECM correspond to electrochemical
35 phenomena in the battery. The first phenomena is the ohmic resistance. It is reproduced in
36 an ECM using the R_o resistor and is the combined resistances of the electrolyte, current
37 collector, active material and separator.[70] It is also influenced by the construction of the
38 battery, the adherence of the active material to the electrode, the electrodes thickness and
39 its area.[71] The first RC_1 element models the impedance of the R_{SEI} layer. SEI formation on
40 the surface of the active material (highlighted in yellow) acts as a barrier for Li-ion
41 intercalation and so creates a resistance (represented by a green line), which can be
42 monitored using EIS. The second RC_2 element models the double layer capacitance (C_{dl}) and
43 charge-transfer (R_{ct}) resistances. Movement of electrons from the electrolyte to the current
44 collector, which is accompanied by a certain amount of resistance, corresponds to R_{ct} in the
45 scheme. When this occurs, a charge boundary is created with opposing polarities
46 (represented by red crosses). C_{dl} occurs at the intersection of the current collector and
47 electrolyte. Two layers of opposing charge, separated by the layer of solvent molecules, are
48 formed between the current collector and electrolyte (represented by a positive red cross
49
50
51
52
53
54
55
56
57
58
59
60

1
2
3 and negative blue line). This difference in charge behaves like a capacitor, and so a capacitor
4 is used in an ECM to model this phenomenon. The Warburg (W) component models the mass
5 transport of Li-ions in the battery using semi-infinite linear diffusion in only one direction. As
6 discussed, C_{dl} , R_{ct} and W impedance appear on the right side of the Nyquist plot, as they are
7 more dominant at lower frequencies. At the highest frequencies, the series resistor (R_0)
8 becomes the most dominant component as ' RC_1 ' and ' RC_2 ' are short-circuited and behave as
9 if they are not present. Extended battery use causes; cell component degradation, electrolyte
10 decomposition, a loss in active material and continual formation of the SEI.[42, 72-74] This
11 occurs even when the battery is not in use and is commonly referred to as calendar
12 ageing.[75] These phenomena reduce the available capacity of the cell and also increase its
13 internal resistance.
14
15
16
17
18
19
20
21
22
23
24
25
26
27

28 **5. Practical Implementation of an AC Impedance Device on a BMS**

29
30 Conventional impedance diagnosis methods are typically time-consuming and involve
31 complex calculations that therefore have limited its on-board applications in battery
32 monitoring. Furthermore, practical integration of EIS on a BMS has historically been hindered
33 by the equipment's large size, power inefficiency and cost [76]. For this reason, EIS has
34 predominately been limited to laboratory conditions with few on-board applications [33, 77,
35 78]. However, recent advances have demonstrated the viability of embedded and scalable EIS
36 devices, effectively solving the size and power-consumption issues of the past. [8, 33-37] EIS
37 measurements are traditionally performed on a battery when it is disconnected from the
38 system and in an offline state. In many battery systems, the battery cannot be turned offline
39 and so it is not desirable to have it disconnected. Therefore, recent studies have attempted
40 to reproduce an EIS version capable of online measurements.[8, 79-82] The main challenge
41 with online EIS measurements is to produce an excitation signal over a wide array of
42 frequencies and then detect the response when other voltages and currents are present.
43 Online EIS measurement methods can be divided into the two general categories of single
44 frequency and multiple frequency acquisition.[83] In the first method, a single frequency
45 sinusoidal signal is injected into the battery and the resultant ac signal is obtained from which
46 the impedance at that single frequency is calculated. This is repeated to extract the total
47
48
49
50
51
52
53
54
55
56
57
58
59
60

1
2
3 battery impedance over a range of frequencies. Although this method can obtain accurate EIS
4 measurements, its acquisition rate is slower than the multiple frequency method. The
5 multiple frequency method injects small ac signals composed of different frequencies into the
6 battery system. By performing Fast Fourier Transform (FFT) calculations on the resultant
7 signals, the impedance at different frequencies can be obtained simultaneously. This method
8 can extract impedances at a faster rate but can be prone to noise interference. Due to this
9 interference the single frequency method is the preferred option in the literature.[23, 29, 30,
10 84, 85]
11
12
13
14
15
16
17
18

19 Implementing EIS using control systems using existing hardware can reduce the cost
20 of equipment and implementation of advanced hardware.[86] For example, Howey *at al.*
21 demonstrated the use of existing power electronics in a vehicle to measure EIS between 1 Hz
22 and 2 kHz.[8] EIS measurements were even obtained using the noise excitation signal
23 generated by a motor controller to produce a perturbation signal. In a similar study, Xia used
24 a square wave perturbation from a DC-DC power convertor to measure the impedance of a
25 battery in a single perturbation period, significantly reducing the overall time needed to
26 perform a measurement.[37] Another study that showed the feasibility of using a power
27 convertor to perturb the cell in order to extract the impedance was performed by Huang and
28 Qahouq.[33] A thorough analysis conducted by Varnosfaderani and Strickland explores in
29 detail the different approaches that have been used in literature for undertaking EIS
30 measurements using existing hardware.[36] These studies demonstrate the viability of
31 embedding and performing online EIS in real-world applications thus validating its potential
32 as a useful tool for estimation of battery states.
33
34
35
36
37
38
39
40
41
42
43
44
45
46
47

48 **6. Reproducibility of EIS and Noise Related Issues**

49 In real-world applications, EIS can be affected by a multitude of noise sources such
50 as electromagnetic interference and electronic switching, which can reduce the quality of
51 the measured data.[1] For example, this is particularly true in an EV, which contains
52 hundreds of individual cells and wire contact points, many metres of wiring, produces large
53 currents, and experiences a great deal of vibration during operation, all of which can
54 introduce uncertainties. This can make the reproducibility of EIS measurements much more
55
56
57
58
59
60

1
2
3 challenging in an onboard application compared to a laboratory setting. Thus, acquiring
4 linear and accurate online impedance data is challenging. Impedance can be acquired when
5 the EV is not in operation however, this may not be suitable for all use cases such as SOC
6 and IT estimation. EV batteries are typically high capacity and have very small impedances.
7 Therefore, a sufficiently large input signal must be produced to reduce the signal to noise
8 ratio (SNR) so an impedance measurement with the necessary accuracy can be acquired.[2]
9 For online measurements, the response signal (typically in the region of 10 mV) needs to be
10 measured over a DC bias that can be an order of magnitude greater. This makes it very
11 challenging to amplify this signal without introducing noise. The use of a large input signal
12 also has implications for the power consumption of onboard EIS hardware. An approach to
13 remove the DC bias current in order to get a more accurate voltage response using a digital
14 servo-loop was proposed by Din et al., which effectively eliminated the DC part of the
15 response and amplified the AC output.[3]

16
17
18 Measurement of noise is unavoidably connected to measuring the voltage response.
19 The ability to quantify and remove this noise is vital for accurate reproducible impedance
20 data. Noise and errors can arise from many external sources as well as the computation of
21 the Fourier transform itself.[4] Further errors can materialise from the battery state
22 estimation models and time variances between the voltage and current measurements. The
23 type of hardware used to measure the impedance on an onboard application, such as an EV,
24 varies with some more susceptible to noise than others. The battery charger[5], motor
25 controller[6] and even the balancing hardware[3] have previously been used to produce a
26 signal capable of estimating the cell impedance. Many methods have been proposed in
27 literature to measure and filter noise. Zhang et al. proposed an online impedance
28 measurement system that could filter out noise using cross-correlation.[7] In this method,
29 both the injected and extracted AC input and output signals are calculated using cross-
30 correlation. From this, the noise at each respective frequency could be filtered out. Howey
31 et al. developed an online impedance measurement system that used the excitation current
32 from the controller of a motor.[6] An approach like this is advantageous as it can help
33 reduce the cost of including dedicated EIS hardware within an EV. The distinguishing feature
34 of this work is the ability to separate the interference from the output signal, thus allowing
35 any noise to be ignored. Another approach used was to ensure the proper calibration of the
36
37
38
39
40
41
42
43
44
45
46
47
48
49
50
51
52
53
54
55
56
57
58
59
60

1
2
3 current and voltage amplifying hardware in order to eliminate any sources of interference
4 from the circuits. A study by Howey et al. compared the online impedance from a
5 commercial Bio-logic VSP potentiostat to an impedance measurement system derived from
6 the existing motor drive in an EV.[8] Like the previous study mentioned, noise was removed
7 using a similar approach. Results indicated that the accuracy of the novel impedance
8 measurement approach was within 2 % RMS for the magnitude part of impedance and 3°
9 for the phase part of impedance compared to the Bio-logic.
10
11
12
13
14
15

16
17 Valid EIS measurements need to be repeatable and noise free. To achieve this,
18 suitable measures can be introduced to minimise the variability in the data. Kramers-Kronig
19 (K-K) relations are a tool that can be employed to assure the accuracy and reproducibility of
20 the acquired impedance.[9] The K-K relations use the relationship between the real and
21 imaginary parts of impedance in order to predict the real part of impedance from the
22 imaginary and likewise, the imaginary part of impedance from the real. This allows any
23 distortions from the real and imaginary parts of impedance to be assessed. Suitable
24 impedance test parameters must also be selected to ensure the EIS test is repeatable. These
25 parameters include the AC amplitude, number of frequencies and points measured and
26 whether the battery is at OCV or if the temperature has recently been altered. A systematic
27 study performed by Pulido et al. assessed the influence of each parameter on the
28 reproducibility of EIS measurements using K-K relations to validate the selection of the most
29 appropriate test conditions.[10] The proposed test method gives valuable insights into how
30 to test for and select the most suitable test parameters for a specific use case. One of the
31 most straightforward approaches is ensuring a test is repeatable by performing multiple
32 measurements and comparing the results. This is both qualitative and quantitative in that
33 each EIS plot must include the same battery processes and the respective values for each
34 must be as similar as possible. Additionally, multiple scans at each frequency can be
35 performed and averaged to decrease the influence of noise, at the expense of time and the
36 amount of power consumed.[11]
37
38
39
40
41
42
43
44
45
46
47
48
49
50
51
52
53

54
55 Allowing a relaxation time before performing an EIS measurement is a common
56 approach used to mitigate the influence from changes in temperature or load.[12] This
57 designated wait period before performing an EIS measurement allows the battery to return
58 to a 'relaxed' state. When no current enters or leaves the cell, polarization of the cell is
59
60

1
2
3 eliminated, which causes a change in the cells voltage as well as its impedance. The time
4 taken to reach this state varies between studies and battery chemistries, but a
5 recommended minimum time of 4 hours is advised.[13] A study by Barai et al. examined the
6 reproducibility of EIS results as a function of relaxation time.[14] In this work, it was
7 discovered that the ohmic resistance was independent of the time allowed for relaxation
8 which enabled it to be used as a consistent parameter for battery state estimation. The
9 charge transfer resistance and double layer capacitance was not reproducible during the
10 first 0 to 10 minutes during relaxation and so it was recommended that they be avoided for
11 any parameter estimation during this time frame. A similar study performed by Messing et
12 al. examined the reproducibility of EIS at various SOCs and temperatures.[15] A model was
13 created to replicate the influence of relaxation on the impedance and was also capable of
14 distinguishing the effect of relaxation from reproducibility errors. Overall, these results
15 indicate that a sufficiently long relaxation time is an effective approach to ensure
16 reproducibility of EIS data however, its suitability for many onboard applications that
17 require online impedance data is limited.

18
19
20
21
22
23
24
25
26
27
28
29
30
31
32 The connections of the wires to and from the battery are an important factor that
33 can influence the impedance measurement also. A study performed by Cheng examined the
34 repeatability of EIS measurements using 5 distinct setups centered around the connection
35 of the wires. It was concluded that the contact resistances of the wires had a large impact
36 on sensing the voltage during the impedance test. Reproducibility was highest when a four-
37 wire connection was used, with the sense and power wires being separated. Contact
38 resistances will generally be higher in an EV compared to laboratory conditions, as battery's
39 in an EV pack or module are typically screwed together in series or parallel connections. As
40 such, it can be difficult to directly connect the sense and power lines from the EIS hardware
41 to the terminals of the battery.[2] This means the measured impedance may differ to that of
42 the battery.

43
44
45
46
47
48
49
50
51
52 Although the ability to extract reproducible impedance data from onboard applications
53 is much more challenging than in a controlled laboratory environment, the work discussed
54 above proves it is indeed possible. A myriad of different approaches and techniques are
55 available to increase the accuracy of the EIS measurement as well as reducing the noise.
56 Furthermore, EIS hardware can be successfully integrated into existing EV power systems
57
58
59
60

1
2
3 without a substantial sacrifice in measurement accuracy. To realise a fully functional BMS
4 that uses impedance for onboard state estimation, much more work is still required to
5 demonstrate the repeatability and accuracy of onboard measurements.
6
7
8
9

10 11 12 **7. Equivalent Circuit Modelling versus Specific Frequencies** 13

14
15 These are the two main approaches that exist in literature when using impedance for
16 battery state estimation. The first involves using battery impedances to update the circuit
17 elements of an ECM, which is then used in conjunction with a model to give the required
18 estimate. A non-linear least squares fitting method is often used to model the EIS data with
19 an ECM [63, 87-92]. This is typically performed a single time prior to cell operation and not
20 repeated and so is usually regarded as an offline method (as EIS is not performed while the
21 battery is under charge or discharge). Many of the ECMs in studies use complex equivalent
22 circuits with constant-phase and Warburg impedance elements.[20, 93-95] However, other
23 studies show that a simple Thevenin equivalent circuit can also achieve similar results.[96-98]
24 While the ECM approach is advantageous, the behaviour of the battery is only characterized
25 at an initial state and so as the batteries behaviour changes, the original ECM values may
26 differ to the current values. Without selection of an accurate and representative fitting model,
27 the accuracy of an ECM will decrease over time.[27, 99, 100]. Additionally, an extensive bank
28 of possible ECM values at different temperatures, SOHs and SOC must be experimentally
29 determined prior to use in order to update the circuit elements, which is a time-consuming
30 and laborious process.
31
32
33
34
35
36
37
38
39
40
41
42
43
44

45 The second approach uses the impedances gathered at specific frequencies to directly
46 infer the batteries state. As the impedance of a battery is a function of SOH, SOC, and IT, at
47 specific frequencies the impedance has been shown to be more dependent on one of the
48 aforementioned parameters while being semi-independent of the rest, thus, allowing the
49 estimation of these parameters.[21, 24, 28, 82, 96, 101-105] This method is normally regarded
50 as being an online method and is performed while the cell is charging or discharging. Online
51 EIS measurements, such as with the specific frequency approach, allow the model to be
52 updated with the most recent impedance values, thus, allowing kinetic processes such as the
53
54
55
56
57
58
59
60

change in temperature to be monitored, something that cannot be typically achieved with the ECM approach.

8. Battery State Diagnosis

8.1. State of Health

SOH is a qualitative measure used to compare the current condition of the battery in relation to its initial condition. [106-108] It is measured in percentage and gives an indication of the age of the battery. A newly manufactured battery has a SOH of 100 %. Once the SOH has decreased to 80 %, the battery has reached its end-of-life (EoL) and needs to be replaced.[109] Knowing the SOH of a battery is essential in determining if the battery can meet the system requirements and informs the user of the capacity available for energy storage.[42, 109] Changes in capacity (Eq. 4) and internal resistance (Eq. 5) are typically used to estimate SOH.[110-112] SOH can also be characterized using a batteries power capability. For example, Ranjbar et al. used the drop-in voltage under load conditions to measure the resistance, enabling the SOH to be calculated using the battery's power.[81]

$$SOH = \frac{Q_{curr}}{Q_{rat}} \quad (4)$$

$$SOH = \frac{R_{curr}}{R_{orig}} \quad (5)$$

where Q_{rat} is the initial capacity of the battery, Q_{curr} is the current capacity, R_{orig} is the original internal resistance of the battery and R_{curr} is the current internal resistance.

The capacity is determined by the electrochemical properties of the battery. This changes over time due to environmental and operating conditions. Battery ageing leads to performance degradation and changes in battery chemistry.[113] LIBs continually degrade during operation and even storage.[42] In high-power applications, such as in an EV, high currents and fast changes between charge and discharge increases the rate of cell ageing.[26, 114-116] In general, the degradation occurs at the interface between the electrodes and

1
2
3 electrolyte.[117] The formation of the SEI layer negatively affects the batteries electrical
4 efficiency and increases resistance.[89] This loss of power and increased resistance results in
5 capacity loss.[26, 118] Other contributing factors are loss of Li-ions and active material caused
6 by formation of the SEI, structural disordering and loss of electrical contact between the
7 current collector and battery material.[119] SOC is measured by examining current and time
8 however, there is no fixed method of calculating SOH.[4] Coulomb counting (CC) is typically
9 the most common SOH estimation techniques. It works by monitoring the charge leaving the
10 cell as a function of time to determine the cells current capacity.[120, 121] By monitoring the
11 change in capacity over time, the SOH can be calculated. Typically, once the capacity of the
12 battery has reduced to 80%, it is in need of replacement. This method is computationally light,
13 only requiring basic addition and multiplication. As a result, CC is well suited for
14 implementation in BMSs. The accuracy of this method depends on the precision of the
15 sensors which need to be periodically calibrated after several battery cycles.[122] This
16 method shows a strong relationship between estimation error and cycle number, with errors
17 up to 10% normal after many cycles. To improve performance, CC is often used in combination
18 with other methods like the Kalman Filter (KF). This combination reduces the estimation error
19 to below 3%, at the expense of a longer calculation time.[45].The KF is a modelling technique
20 often used in battery state estimation. The complexity of this method lies somewhere
21 between medium and high, thus it has seen limited implementation on commercial BMS. As
22 batteries are non-linear systems, modified versions of the KF are proposed in literature for
23 SOH estimation. Both Rosca et al. and Andre et al. used an Extended Kalman Filter (EKF) in
24 combination with a second-order Randles circuit for SOH estimation.[106, 110] In the first
25 case, SOH is estimated using the battery SOC and in the second case the model uses battery
26 impedance. Daboussy et al. used an EKF to model the parameters of a LIB used in automotive
27 applications.[123, 124] The experiment showed a SOH estimation error of less than 1%. A
28 model using an Unscented Kalman Filter (UKF) in combination with a second-order Randles
29 circuit was proposed by Andre et al. for the estimation of SOH.[125] A UKF is desired as it
30 eliminates some of the drawbacks associated with an EKF.[126] In general, the estimation
31 error for Kalman filtering is lower than that of the CC and Open-circuit Voltage (OCV) methods
32 when used individually, achieving errors below 3 %.[45] Other estimation methods include
33 Artificial Neural Networks (ANN) and Fuzzy Logic (FL) approaches. The main advantage of
34 using an ANN is its ability to learn and adapt by merging new experimental data. ANNs are
35
36
37
38
39
40
41
42
43
44
45
46
47
48
49
50
51
52
53
54
55
56
57
58
59
60

very accurate with a study performed by Ungurean et al. showing a maximum estimation error of 2 % for SOH estimation.[45] Despite its potential, ANNs are computationally demanding which may be an issue when trying to implement them on a BMS.[2] The FL method is a powerful technique used to model non-linear systems without needing a mathematical model.[127] Singh et al. used this method, in combination with data acquired from impedance spectroscopy, to develop a FL SOH estimation model. [128] Results indicated the method achieved an estimation accuracy within $\pm 5\%$. One of the main disadvantages of this method is that it requires a large volume of test data and is computationally intensive thus limiting its real-time practical use in a BMS. The estimation accuracy of this method is average, with errors ranging between 1.4 % and 10 %.[45]. Current estimation techniques lack the accuracy or are too complex, limiting their practicality in real-world applications, hence why the SOH function is not available on a large portion of BMSs. EIS is seen as a promising diagnostic tool that offers enhanced precision and monitoring capabilities, to derive an impedance model capable of accurately estimating the SOH of a LIB. It must be noted that while SOH can be used as an indicator that a battery has reached its end-of-life, the battery still may be suitable for other secondary applications, hence the term 'second-life applications'.

8.1.1 State of Health Estimation via Impedance

Recently, more emphasis has been placed on EIS as a useful tool in measuring battery SOH and remaining-useful-life (RUL). EIS has been shown to reveal changes in the cells electrochemical processes as it ages.[80, 129] As the battery ages, the value of the ECM components change as different parts of the cell are degraded or its chemistry altered. These changes are outlined in Table 1.

ECM Component	Unit	Degradation Mode	Potential ageing mechanism	Observed effects
Increase in R_{ohm}	(Ω)	Conductivity loss	- Corrosion of current collector - Decomposition of binder	PF CF
Increase in R_{SEI} & R_{ct}	(Ω)	Loss of Lithium	- Electrolyte decomposition - Oxidation of electrolyte	CF & PF PF

			- Lithium plating	CF & PF
			- Formation of lithium grains	CF & PF
			- Solvent co-intercalation	CF & PF
Increase in R_w	(Ω)	Loss of active material	- Electrode decomposition	CF & PF
			- Oxidation of electrolyte	CF & PF
			- Formation of lithium grains	CF
			- Solvent co-intercalation	CF & PF
			- Transition metal dissolution	PF

Table 1. Relationship between ECM components, the ageing mechanism and what effect is observed; Power Fade = PF; Capacity Fade = CF.[91]²

SOH determinations via EIS have been widely used to correlate the rise in battery impedance to the loss in capacity.[10, 26, 27, 101, 130, 131] This is performed by analysing acquired impedance spectra, typically using an ECM. The variation in the ECM elements is then used to monitor the ageing processes within the cell. Stroe *et al.* compared the Nyquist plots of fresh unused batteries to batteries that had undergone accelerated ageing.[23] Data from these plots were fitted using an ECM and resistive and capacitive values were shown to increase as the battery aged. The increase in ohmic resistance as the battery aged was correlated to a decrease in the LIBs pulse power capability. Similar offline approaches with ECMs have been used in other studies. Yuan demonstrated that charge-transfer resistance showed good correlation with battery degradation.[132] To achieve a low estimation error, only impedance data between 30 % - 60 % SOC was used, as this zone showed the least influence of SOC and the greatest influence of SOH on predictions. This method achieved an estimation error of 6.1 % over long-term cycling. Galeotti *et al.* examined the behaviour of battery ohmic resistance at various SOCs and cycle numbers to create a look-up diagnostic map to act as a standard to which other batteries of the same chemistry would be compared (Fig. 5a).[26] An ECM to fit impedance data and the theory of evidence model were then applied, achieving a maximum SOH error of 3.73 % with standard cells and 8.66 % with anomalous cells. The intrinsic relationship between ohmic internal resistance and capacity

² Reprinted from The Journal of Power Sources, Vol. 360, Carlos Pastor-Fernández, Kotub Uddin, Gael H.Chouchelamane, W. Dhammika Widanage & James Marco, A Comparison between Electrochemical Impedance Spectroscopy and Incremental Capacity-Differential Voltage as Li-ion Diagnostic Techniques to Identify and Quantify the Effects of Degradation Modes within Battery Management Systems, Pages 301-318., Copyright (2017), with permission from Elsevier.

was used by Chen et al. to estimate battery capacity which were then used to determine SOH (Fig. 5b).[133] The proposed method required a full discharge at the start and at a random future point to correlate the ohmic internal resistance with the fade in capacity. Impedance data between 30 % – 80 % SOC was used, as the error between SOC values was lowest between these points. The maximum error reported, between capacity fade (used as a reference) and the increase in ohmic internal resistance, was less than 4 %.

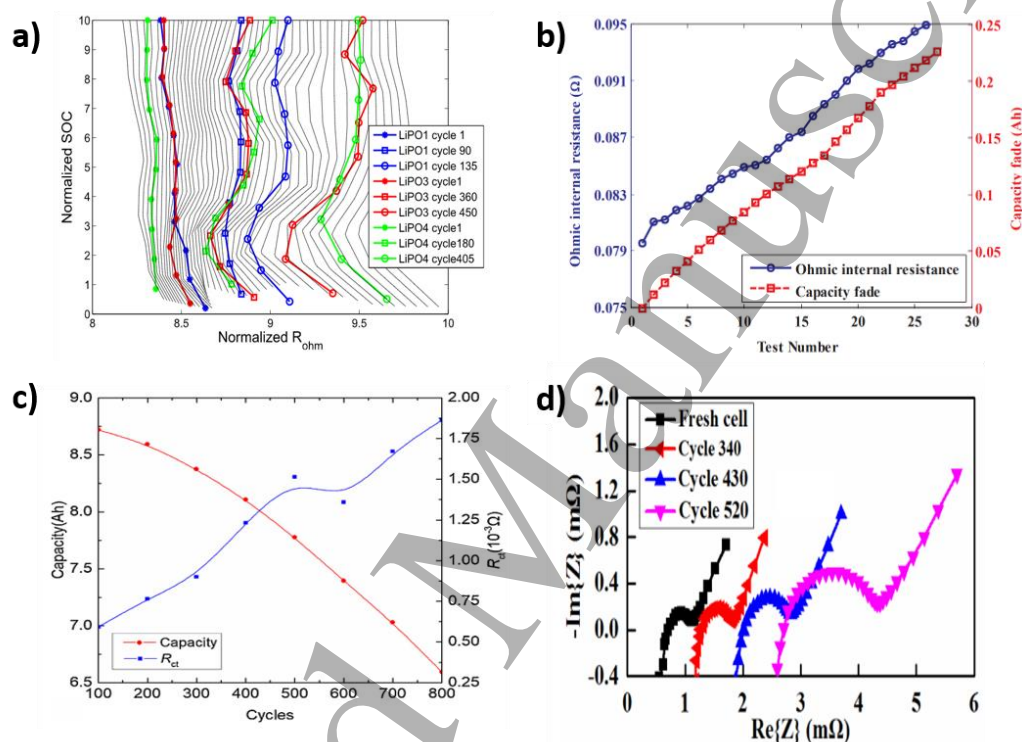


Fig. 5. a) Diagnostic map used for SOH estimation. The black lines represent reference batteries and the tested batteries are in coloured lines.[26]³ b) Graph showing the relationship between the rise in ohmic resistance and capacity fade.[133]⁴ b) Impedance spectra at different cycle number and ageing states.[131]⁵ d) Comparison of the capacity and charge-transfer resistance as a function of cycle number.[134]⁶

³ Reprinted from Energy, Vol. 89, Matteo Galeottia, Lucio Cinà, Corrado Giammanco, Stefano Cordiner & Aldo Di Carlo, Performance analysis and SOH (state of health) evaluation of lithium polymer batteries through electrochemical impedance spectroscopy, Pages 678-686, Copyright (2015), with permission from Elsevier.

⁴ Reprinted from Measurement, Vol. 116, Lin Chen, Zhiqiang Lü, Weilong Lin, Junzi Li & Haihong Pan, A new state-of-health estimation method for lithium-ion batteries through the intrinsic relationship between ohmic internal resistance and capacity, Pages 586-595, Copyright (2018), with permission from Elsevier.

⁵ Reprinted from Journal of Energy Storage, Vol. 21, Xueyuan Wang, Xuezhe Wei & Haifeng Dai, Estimation of state of health of lithium-ion batteries based on charge transfer resistance considering different temperature and state of charge, Pages 618-631, Copyright (2019), with permission from Elsevier.

⁶ Reprinted from Energy Procedia, Vol. 105, Jiuchun Jiang, Zhisong Lin, Qun Ju, Zeyu Ma, Caihui Zheng & Zhanguo Wang, Electrochemical Impedance Spectra for Lithium-ion Battery Ageing Considering the Rate of Discharge Ability, Pages 844-849, Copyright (2017), with permission from Elsevier.

1
2
3
4
5
6 The use of ohmic resistance for SOH estimation is well documented in literature. Jiang
7 *et al.* [134] examined the correlation between ohmic resistance and cycle number and
8 reported that ohmic resistance increased as the battery was cycled (Fig. 5c). This is supported
9 by Wang *et al.* [131] who found that the impedance curve on a Nyquist plot moves further to
10 the right as a battery aged, indicating an increase in resistance (Fig. 5d). Other impedance
11 parameters that have been used to estimate SOH include the zero crossing frequency of
12 battery impedance phase [82], the magnitude of impedance at 5.6 Hz and 10 Hz and the phase
13 angle at 3.16 Hz [135], the shape of the Nyquist plot [103] and single frequency points.[136]
14 Although many studies validate the use of EIS to determine SOH, tests are typically performed
15 in at OCV i.e. the batteries is left offline long enough so that all transient charge / discharge
16 processes are minimised, which is not always applicable in real-world scenarios. Additionally,
17 identical accelerated ageing tests at constant temperatures does not adequately replicate the
18 variable environmental conditions LIBs operate in real world conditions. Analysing the data in
19 full, we can see that the error for impedance based SOH estimation lies below 10 %, with most
20 methods averaging 3 – 7 % error. Studies differ in quoting the accuracy in terms of maximum
21 error, average error, MSE or depicted graphically. Others discuss important trends linking
22 particular parts of impedance to SOH. Compared to existing methods of SOH estimation (Fig.
23 6), we see that EIS based SOH estimation is comparable in accuracy, with the average
24 estimation accuracy for experimental techniques being approximately 94 % and adaptive
25 methods approximately 96 %.[137] The accuracy of some approaches, such as neural
26 networks and big data, are high but require a large amount of computational power, which
27 limits their application. Impedance is a relatively easy experimental technique to perform and
28 demonstrates high SOH estimation accuracies, thus validating its use as a potential onboard
29 SOH estimator.
30
31
32
33
34
35
36
37
38
39
40
41
42
43
44
45
46
47
48
49
50
51
52
53
54
55
56
57
58
59
60

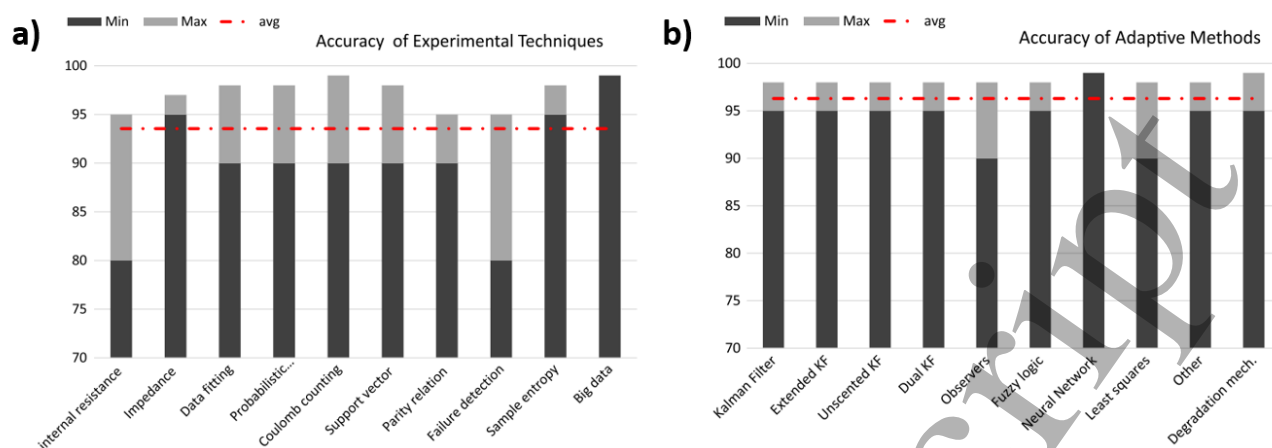


Fig. 6. Graphs showing the minimum, maximum and average estimation accuracies for SOH estimation using a) experimental techniques and b) adaptive methods.[137]⁷

⁷ Reprinted from Renewable and Sustainable Energy Reviews, Vol. 56, Maitane Berecibar, Iñigo Gandiaga, Igor Villarreal, Noshin Omar, Joeri Van Mierlo & Peter van den Bossche, Critical review of state of health estimation methods of Li-ion batteries for real applications, Pages 572-587, Copyright (2016), with permission from Elsevier.

Author(s)	Battery Chemistry	Part of Impedance	F (Hz) for Model	Model	Accuracy
Haiying et al.[138]	LFP	ECM	1 – 100 Hz	ECM	Unspecified
Zenati et al.[139]	NCA	Nyquist plot	0.1 Hz - 65 kHz	FL	Unspecified
Eddahech et al.[130]	NMC	ECM	0.1 Hz - 10 kHz	ECM / RNN	MSE = 0.462
Eddahech et al. [101]	NMC	Z' at 0.1 Hz	0.1 Hz	ECM / GA	Depicted graphically
Stroe et al.[23]	LFP	ECM	0.01 Hz - 10 kHz	ECM / GA	Unspecified
Galeotti et al.[26]	LiPo	R _o	0.2 Hz - 5 kHz	ECM / ToE	Max. error of tested/untested cell = 3.73 % & 8.66 %
Xia[82]	LCO	F ₀ phase	1 Hz – 20 kHz	ANN	Unspecified
Mingant et al.[103]	LFP:LTO	ECM	0.01 Hz – 100 kHz	ECM / LS / PF / LR	Error = 7 %
Love et al.[136]	LCO	Z' at 316 Hz	0.01 Hz – 50 kHz	GA	Unspecified
Wang et al.[140]	LFP	Z' at 10 kHz	0.01 Hz – 1 kHz	Interpolation Map	Unspecified
Wang et al.[131]	LFP	R _{ct}	0.01 Hz – 1 kHz	ECM / CPSA / GA	Absolute error = <15%
Zhou et al.[27]	NMC	R _o , R _c & R _{sei}	Determined via TC	DRT	Error = <10 %
Zhang et al.[28]	LCO	Z' & Z'' at 17.80 Hz & 2.16 Hz	0.02 Hz – 20 kHz	GPML	Depicted graphically
Yuan [132]	LFP	R _{ct}	-	ECM / TPE	Error = 6.1 %
Chen et al. [133]	NMC	R _o	-	ECM / RLS	Max error = ±4 %
Jiang et al. [134]	LMO / LMNO	Φ, R _{tot} , R _{ct} & R _o	0.01 Hz – 1 kHz	-	Unspecified
Kassem et al. [84]	LFP	R _{tot} , R _o , R _{ct} & W	0.01 Hz – 10 kHz	-	Unspecified

Table 2. Comparison of studies that used impedance measurements to determine battery SOH; Z' = real impedance; Z'' = imaginary impedance; Z = magnitude; φ = phase; R_o = ohmic resistance; R_{ct} = charge-transfer resistance; F₀ = intercept frequency; R_c = contact resistance; R_{sei} = SEI resistance; DRT = distribution of relaxation time; W = Warburg impedance; RLS = recursive least squares; RLS = recursive least squares; RNN = recurrent neural network; LR = linear regression; PF = polynomial fitting; CPSA = chaotic particle swarm algorithm; GPML = Gaussian process machine learning; TC = time constants; TPE = three point extraction; R_{tot} = total impedance; Φ = phase

8.1.2 Fault Detection

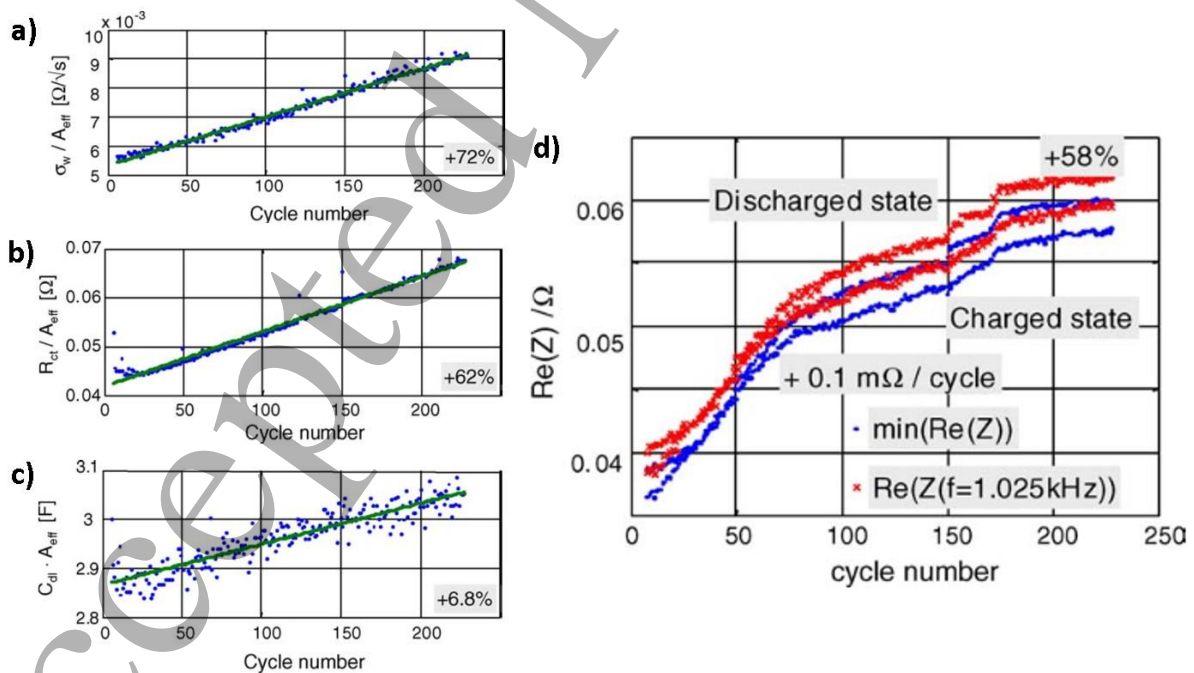
Safety is a critical parameter in all battery systems. The failure of a LIB has been reported to be 1 in 40 million if used and stored correctly.[141] However, overcharging & over discharging, high or low temperatures and physical damage can increase the rate of failure.[142] Commercial LIBs have safety mechanisms, such as voltage and temperature cut-offs, however large scale battery accidents have occurred which resulted in large scale recalls. The root cause of the accidents include excessive heating, short-circuits, overcharging, overdischarging and physical damage.[143] Due to these dangerous occurrences, strict rules regarding the transport of LIBs have been implemented. For example, all LIBs must now have a SOC less than 30 % to be shipped via aircraft.[144]

The consumer demand for smaller portable electronic devices further drives the increase in LIB energy density, which has the potential to cause more serious safety incidents. The lessons of past incidents has clearly demonstrated that LIB safety technology needs to be further developed. Hence, the importance of developing a more sophisticated and advanced failure detection methods cannot be emphasized enough. In-situ monitoring of battery impedance can be used to gain greater insight into battery ageing mechanics.[145] Extending this knowledge to battery failure detection can improve the functional safety of battery powered devices. Faults in LIBs are typically caused by the ageing process or physical / electrochemical abuse and are expressed by an increase in internal impedance and a loss in capacity.[146] The majority of studies on battery parameter estimation over the last twenty years has focused on the big three, which are SOC, SOH and IT estimation, however limited research is available regarding EIS for fault detection.

8.1.3 Fault Detection Methods

Faults are usually diagnosed when some variables in the battery present behaviours different from ordinary use. Through the use of a model, the difference between regular battery behaviour and measured battery behaviour can be diagnosed for fault detection. The simplest form of failure detection sets a safety threshold, that if exceeded a fault occurs. Kaypmaz and Tuncay demonstrated this through the use of an ECM whose parameters were extracted through ac impedance spectroscopy.[147] Initial testing on

normal cycled, overcharged and overdischarged batteries was performed to identify the effect this had on the ECM parameters. A FL model then analysed the difference in values between initial conditions and test conditions using three inputs, ΔR_0 , ΔR_{ct} and ΔC_{dl} . A safety threshold was then formulated based on the difference in values between the normal cycled battery and the overcharged and overdischarged batteries. A similar approach was conducted by Singh *et al.* where overcharge and overdischarge cycles were examined and a model was constructed for normal operation and any other operation that exceeded normal limits.[148] Impedance data along with an ECM was used to construct a battery model. Multiple model adaptive estimation was adopted for comparing the measured data against each separate model derived for battery overcharge and overdischarge. Simulations of battery fault scenarios indicate that this method could detect battery faults in real-time. For example, online EIS measurements were used by Troltsch *et al.* to update an ECM as the battery cycled and was able to characterize battery ageing dynamics, such as R_{ct} , R_o and the W coefficient, which showed high sensitivity to changes in battery capacity. Over 230 cycles, the R_{ct} , R_o , C_{dl} and W coefficient increased 62 %, 58 %, 6.8 % and 72 % respectively from their initial values (Fig. 7).[89]



1
2
3 **Fig. 7.** Graphs showing the migration of a) Warburg resistance, b) charge-transfer resistance,
4 c) double-layer capacitance and d) series resistance versus cycle number for a LCO Li-ion
5 battery.[89]⁸
6
7
8
9

10 The effectiveness of a fault detection system depends on its ability to acquire up to
11 date data, so an online method such as this is highly desirable. Signal processing methods,
12 like EIS, can monitor in real time the dynamic behaviour of the battery something which is
13 lacking in model-based methods. Carkhuff *et al.* designed an online impedance-based
14 multicell BMS for safety monitoring using the correlation between specific frequency ranges
15 and the following parameters: (1) temperature estimation of the anode using the phase shift
16 at 70 Hz, (2) temperature estimation of the cathode using the phase shift at 10 Hz, (3) real
17 impedance from 1000 Hz to 400 Hz for the resistance of the electrolyte and SOH, (4) real
18 impedance at 2 Hz for SOC. [24] The impedance-based BMS was successful in detecting cell
19 mismatches and real time monitoring of the IT of the battery pack. This is significant as
20 traditional BMSs, that monitor the voltage and voltage and surface temperature of LIBs, do
21 not succeed in identifying cell mismatches and emerging failures that can occur due to
22 overcharging, overdischarging, short circuiting and even calendar ageing. Prediction of a
23 mismatched cell is crucial for a battery's electrical efficiency and thermal management.[24]
24 Love and Swider-Lyons developed an impedance based diagnosis method for detecting the
25 overcharging of batteries using a single frequency measurement at 500 Hz.[85] This simple
26 and quick approach of fault detection could clearly detect changes in the impedance spectrum
27 in the real and imaginary domains at voltages higher than 4.2 V. Additionally, results suggest
28 that this trend is independent of battery size. A hybrid approach between battery models and
29 signal processing methods is perhaps the best design as it enables the processing power of a
30 model and the online acquisition of data to update said model to better diagnose faults faster
31 and more accurately. Table 3 lists existing studies that used impedance for fault detection.
32
33
34
35
36
37
38
39
40
41
42
43
44
45
46
47
48
49
50
51
52
53
54
55
56
57

58
59 ⁸ Reprinted from *Electrochimica Acta*, Vol. 51/8-9, Uwe Tröltzsch, Olfa Kanoun & Hans-Rolf Tränkler , Characterizing aging
60 effects of lithium ion batteries by impedance spectroscopy, Pages 1664-1672, Copyright (2006), with permission from
Elsevier.

Author(s)	Chemistry	Part of Impedance	F (Hz) for Model	Model	Accuracy
Kaypmaz & Tuncay [147]	NMC	$R_0 / R_{ct} / C_{dl}$	0.05 Hz – 5 kHz	ECM / FL	Unspecified
Singh et al. [148]	LFP	ECM	Determined via ECM	ECM / KF / MMAE	Unspecified
Troltsch et al. [89]	LCO	$R_s / R_{ct} / C_{dl} / W$	0.03 Hz - 10 kHz	ECM	Unspecified
Carkhuff et al. [24]	NCO	ϕ at 10 Hz & 70 Hz / Z' from 400 Hz to 1000 Hz / Z' at 2 Hz	1 – 1000 Hz	SFP	Unspecified
Love & Swider-Lyons [149]	LCO	Z' & Z'' at 500 Hz	0.05 Hz - 50 kHz	NP	Unspecified

Table 3. Comparison of studies that used impedance measurements for fault detection; MMAE = multiple model adaptive estimation; NP = Nyquist plot; SFP = single frequency point; R_s = series resistance.

8.2 Internal Temperature

Thermal monitoring of LIBs, especially in battery packs comprised of many cells, is of crucial importance for the BMS.[150] The emerging use of LIBs in EVs and stationary energy storage has increased the demand for higher capacity batteries and the need for faster charging and discharging, which can cause battery temperatures to rise substantially.[30, 151] Management of LIB temperature in EV applications is an important issue for LIBs because of their limited operating temperature range (5 - 45 °C for charge and -10 - 55 °C for discharge).[152] The ability to accurately measure the internal cell temperature is paramount for its safety, performance and longevity as extremes in either the high or low ends can trigger failure of the battery with hazardous consequences.[153] Overheating can cause excessive exothermic reactions, such as electrolyte decomposition, dissolution of the SEI layer and electrode active material potentially causing a catastrophic thermal runaway.[150, 154-159] Furthermore, it has been shown that an increase of one degree of temperature between 30 - 40°C, a LIBs lifespan is reduced by two months.[160] On the other hand, operation in low temperatures can be just as damaging, most notably during charging, where limitations on Li-ion mass transport can cause plating of Li metal on the anode contributing to a decrease in

1
2
3 available capacity and possibly battery failure.[155, 161-164] Therefore, the IT of a LIB, which
4 cannot be directly measured, is extremely valuable for operating LIBs safety.[47] In practice,
5 the surface temperature of a LIB is the only measureable areas, however, it is the internal
6 battery temperature that determines the performance of a LIB.[165] Simply measuring the
7 surface temperature of the battery is inadequate under normal operating conditions, such as
8 the standard charge / discharge cycle in an EV, as the battery internal temperature can heat
9 up much faster than the surface temperature. As such, the difference in temperature
10 between the cell surface and core can vary by as much as 10 °C.[165] While such an incident
11 is rare, inaccurate monitoring of a battery can result in safety issues and possible recall of the
12 battery powered device. Therefore, it is of utmost importance to acquire an accurate
13 estimation of the IT of a LIB during operation to prevent the occurrence of a hazardous event.
14
15
16
17
18
19
20
21
22
23

24 As heat generation within a battery is a complex electrochemical process,
25 understanding how the charge and discharge rate of a battery will affect its temperature is
26 especially important.[166] Existing BMSs typically use surface mounted temperature sensors
27 or thermistors in tandem with a thermal model to estimate internal cell temperature.[46,
28 167] Rapid changes in IT may not register with surface mounted sensors, meaning it may not
29 be possible to detect the onset of a thermal runaway under normal operating conditions.[168]
30 Therefore, the ability of this method to measure internal cell temperature in all conditions is
31 lacking. Furthermore, large battery packs, like those found in an electric vehicle, contain
32 hundreds if not thousands of cells, thus, placing a surface temperature sensor on each
33 represents a substantial cost and so thermal management is typically performed with a
34 module rather than an individual cell.[169] For this reason, fewer temperature sensors are
35 employed in battery packs than the optimum required. For example, a Chevrolet Volt uses 16
36 temperature sensors to manage 288 cells and a Toyota Prius uses 42 for 288 cells.[170] Many
37 different thermal models of varying complexities and accuracy's have been proposed in
38 literature. Thermal models, for individual cells and battery packs, have been developed that
39 consider heat generation and dissipation processes outside and within the battery.[171-174]
40 Although these proposed models show good accuracy, the complexity is extremely high which
41 limits its use in onboard applications. Additionally, it is challenging to measure the chemical
42 and physical parameters needed for these models. To better measure the heat generation
43 inside the core of a Li-ion battery, some researches have installed thermocouples directly
44
45
46
47
48
49
50
51
52
53
54
55
56
57
58
59
60

1
2
3 inside the battery.[175, 176] Due to increased cost and safety considerations, this approach
4 is not appropriate for industrial applications but does help elucidate the core temperature
5 heating effects.[174] A combination of a thermal and electrochemical model have been
6 proposed that use equations that model internal battery thermal-electrochemical processes
7 however, these type of models are not suitable for online applications.[174, 177, 178] The
8 widely adopted ECM often models the temperature effect on resistive and capacitive
9 components. However, the surface temperature of the battery is only used in most papers,
10 as it is directly measureable.[179, 180]
11
12
13
14
15
16
17
18
19

20 8.2.1 Internal Temperature Estimation via Impedance

21
22
23 Considering the growing trend of cell level supervision in battery packs, instead of
24 using multitudes of surface mounted external temperature sensors, the IT can be estimated
25 using online EIS, using the intrinsic relationship between the battery impedance and internal
26 temperature [12, 21, 22, 29, 30, 32, 105, 150, 181, 182]. Impedance-based temperature
27 estimation is a new approach that may acquire faster estimated of temperature than existing
28 methods.[183] Monitoring the IT of LIBs has been widely reported in literature for a wide
29 range of LIB chemistries and geometries.[150] Work by researchers such as Srinivasan [21,
30 184, 185], Schmidt [22, 186, 187] and others [12, 29, 30, 163, 188, 189] have demonstrated
31 the connections between battery IT and various parameters derived via EIS. Correlating
32 impedance to IT typically takes advantage of the properties of the SEI layer which does not
33 store any charge itself and so is largely unaffected by the batteries SOC [21, 22, 163, 164, 188-
34 191]. Therefore, as long as a stable SEI is present, an accurate IT estimate can be achieved by
35 analysing the battery impedance at specific frequencies to estimate the cell temperature
36 without the need for a thermal model or temperature sensor.[12, 21, 22, 32, 184] For this
37 reason, EIS is often referred to as 'sensorless' as no surface-mounted or internal sensors are
38 needed.[29, 32] Additionally, EIS avoids the heat transfer delay associated with surface
39 temperature measurements due to the batteries thermal mass.[29] Srinivasan *et al.* was the
40 first to propose using EIS as an internal battery temperature estimator.[21] This work
41 demonstrated an intrinsic relationship between battery impedance at specific frequencies
42 (specifically the phase between 40 Hz – 100 Hz) and battery IT. This frequency range was
43 chosen as it is dominated by the anode and therefore is unaffected by structural changes to
44
45
46
47
48
49
50
51
52
53
54
55
56
57
58
59
60

1
2
3 the cathode.[189] This is important as cell degradation under normal conditions is primarily
4 caused by the cathode, thus the stable anode structure enables accurate temperature
5 estimation even after hundreds of cycles.[21, 90, 192, 193] Furthermore, the impedance of
6 the SEI layer on the anode has been shown to be highly sensitive to changes in temperature
7 and independent of SOC.[21, 193] Using this relationship, online temperature measurements
8 were acquired, even when the battery was under load. The defining characteristic of this
9 method is the use of a single frequency, in contrast to a full range of frequencies to determine
10 battery IT, enabling a near instantaneous acquisition of data.[150] Troxler *et al.* demonstrated
11 that temperature non-uniformity in a cell could be accurately modelled by representing the
12 battery as a connection of individual parallel electrodes and using electrochemical impedance
13 to update these parameters.[194] The charge-transfer resistance of the battery was shown
14 to have a strong temperature dependence that obeyed Arrhenius law. Unlike Srinivasan, who
15 used the phase shift of the battery in his model, Schmidt *et al.* showed that the real
16 impedance could also be used to estimate the cell temperature of a prismatic pouch-cell (Fig.
17 8a).[22] A higher frequency range of 10.3 kHz was chosen based on empirical analysis which
18 showed that very high frequencies mitigated the dependence of SOC on the temperature
19 estimation. A temperature estimation error of 0.17°C was achieved when the SOC was used
20 and 2.5 °C when the SOC wasn't used in the model. More recently, attempts have been made
21 to identify the optimal impedance range to infer temperature. Raijmakers *et al.* used the
22 intercept frequency, which is the frequency at which the imaginary impedance is zero, to infer
23 temperature.[29] This point decreased as the temperature increased and was strongly
24 independent of battery SOC and SOH as seen in Fig. 8b to 8d. Wang *et al.* discovered that the
25 phase impedance at 79.4 Hz is highly sensitive to changes in temperature by examining the
26 change in impedance at 0 °C, 23 °C and 45°C.[140]
27
28
29
30
31
32
33
34
35
36
37
38
39
40
41
42
43
44
45
46
47
48
49
50
51
52
53
54
55
56
57
58
59
60

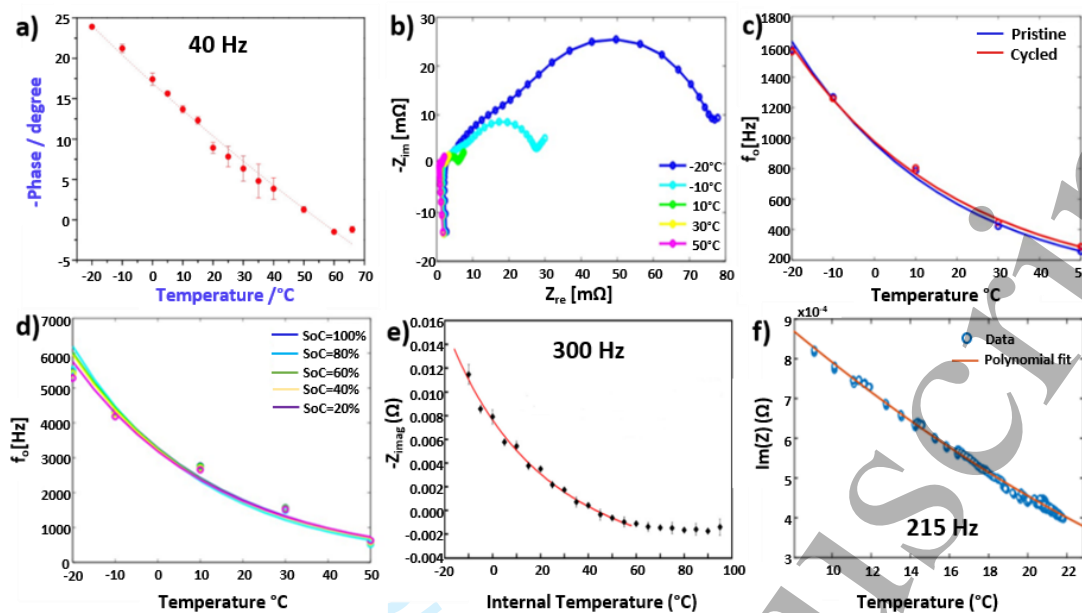


Fig. 8. a) Variation of the phase shift at 40 Hz vs. temperature.[21]⁹ b) Impedance spectra of a NCA battery at temperatures ranging from -20 °C to 50 °C.[29]¹⁰ c) The intercept frequency as a function of temperature for a unycled and cycled NCA battery.[29] d) Intercept frequency as a function of temperature for a unycled LFP battery at various SOCs.[29] e) Plot of average Z_{imag} at 300 Hz at all SOCs as a function of internal temperature.[150]¹¹ f) Change of Z_{imag} at 215 Hz with temperature.[167]¹²

Temperature estimation using impedance up to this point had only been validated for cell temperatures up to a maximum of 66°C, above which the accuracy decreased significantly.[195] Spinner et al. demonstrated improved estimation accuracies in the temperature range 68 °C – 95 °C using the imaginary impedance at 300 Hz and the use of a secondary empirical fit (Fig. 8e).[150] Investigation of the sensitivity of various impedance regions to temperature and other state parameters such as SOC and SOH was performed by Koch and Jossen.[182] It was found that the real and absolute impedance values show a

⁹ Reprinted from *Electrochimica Acta*, Vol. 56/17, Rengaswamy Srinivasan, Bliss G. Carkhuff, Michael H. Butler & Andrew C. Baisden, Instantaneous measurement of the internal temperature in lithium-ion rechargeable cells, Pages 6198-6204, Copyright (2011), with permission from Elsevier.

¹⁰ Reprinted from *Journal of Power Sources*, Vol. 247, L.H.J. Rajmakers, D.L. Danilov, J.P.M. van Lammeren, M.J.G. Lammers & P.H.L. Notten, Sensorless battery temperature measurements based on electrochemical impedance spectroscopy, Pages 539-544, Copyright (2014), with permission from Elsevier.

¹¹ Reprinted from *Electrochimica Acta*, Vol. 174, Neil S. Spinner, Corey T. Love, Susan L. Rose-Pehrsson & Steven G. Tuttle, Expanding the Operational Limits of the Single-Point Impedance Diagnostic for Internal Temperature Monitoring of Lithium-ion Batteries, Pages 488-493, Copyright (2015), with permission from Elsevier.

¹² Reprinted from *Journal of Power Sources*, Vol. 327, Robert R. Richardson, Shi Zhao & David A. Howey, On-board monitoring of 2-D spatially-resolved temperatures in cylindrical lithium-ion batteries: Part II. State estimation via impedance-based temperature sensing, Pages 726-735, Copyright (2016), with permission from Elsevier.

1
2
3 strong dependency on SOC, relative to the imaginary and phase shifts, thus the latter were
4 recommended for monitoring battery temperature.[195] The optimal frequency ranges were
5 also evaluated using similar criteria. Richardson *et al.* demonstrated the suitability of EIS for
6 rapid estimation of IT using the real impedance at 215 Hz (Fig. 8f). [167] Error analysis of this
7 approach found an average RMSE of 0.275 °C across 8 different cells. When compared to
8 conventional methods used for temperature estimation, usually surface thermocouples, the
9 accuracy of EIS based methods are slightly inferior; however, the reduction in cost and its
10 simplicity may justify its use in commercial systems, such as an EV. [196] Beelen *et al.*
11 performed an accuracy comparison of existing methods in literature using Monte Carlo
12 simulations, where EIS was used for temperature estimation.[32] From this analysis, a new
13 model was suggested, which demonstrated improved temperature estimation accuracy
14 based on an analysis of the experimental design and frequency's used in existing studies. Low
15 temperature impedance analysis from -60 °C to 25 °C was performed by Zhang where the
16 effect on the impedance parameters R_{ct} , R_{sei} and R_b was monitored. At low temperatures,
17 R_{ct} showed the greatest increase and was determined to be the main limiting factor that
18 affected the low temperature performance of LIBs.[163] Table 4 lists existing studies that use
19 impedance for temperature estimation, the frequencies used and the cell chemistry.[195] A
20 myriad of different metrics were used in each study, with no underlining consensus on which
21 is the most optimal. Existing studies have been limited by the small volume of batteries and
22 standard cycling conditions (constant current) that do not mirror real-world usage (variable
23 currents). Additionally, small sample sizes may not fully account for the non-uniformities and
24 differences seen between individual batteries of the same chemistry and type. Battery
25 imaginary impedance is the most common metric used for IT estimates as well as the 40 Hz
26 to 500 Hz frequency range that typically correlates with the anode impedance, and in
27 particular the SEI layer. The average estimation error for EIS based temperature estimation
28 across all studies was extremely low at 1.30 °C. A key advantage of EIS, setting it apart from
29 other existing methods, is its ability to estimate the average IT of the battery, where other
30 methods typically use surface temperature analysis. This can be deemed beneficial, as it does
31 not require the addition of a hardware temperature sensor, thus lowering the
32 implementation cost. Additionally, EIS is capable of estimating the other battery states, such
33 as SOC and SOH, and so it an attractive option. Thermal modelling of LIBs has been reported
34 to achieve accuracy's in the 1 – 2 °C range.[197] While accurate, thermal models are
35

1
2
3 computationally intensive, which limits their integration into some energy storage systems.
4
5 Furthermore, accurate knowledge of all LIB physical properties is required to ensure accurate
6
7 temperature estimation.
8
9
10
11
12
13

Author(s)	Battery Chemistry	Temp (°C) examined	F (Hz) for Model	Part of impedance	Model	Accuracy
Troxler et al.[194]	NMC	-13 to 55	GA	R_{ct}	ECM	Unspecified
Srinivasan et al.[184]	LFP	-20 to 66	40 Hz	ϕ	None	Unspecified
Beelen et al.[32]	NMC	-20 to 50	133 Hz & 630 Hz	Z' & Z''	MC	Absolute error = 0.4 °C
Raijmakers et al.[29]	LFP / NCA	-20 to 50	-	F_0	None	Unspecified
Wang et al.[140]	LFP	0 to 45	79.4 Hz	ϕ	Interpolation map	Unspecified
Zhu et al.[12]	LFP	-20 to 50	10 Hz, 50 Hz & 100 Hz	ϕ & Z	Look-up table	Unspecified
Richardson et al.[198]	LFP	-20 to 45	215 Hz	Z'	TM	RMSE = 1.35 °C (core) & 1.34 °C (surface)
Hausmann et al.[199]	PHEV	0 to 40	500 Hz	Z'	GA	Unspecified
Richardson et al.[167]	LFP	~ 8 to 30	215 Hz	Z'	TM / EKF / PF / DEKF / DKF	Error = 0.1 °C to 0.7 °C
Raijmakers et al.[200]	LFP	-20 to 50	-	NZIF	GA	Depicted graphically
Spinner et al.[150]	LCO	-20 to 95	300 Hz	Z''	LS / LC	Error = 3 °C to 7 °C
Li et al.[201]	LCO	-40 to 0	1-100 Hz	Z'	TM / ECM	Error = 1 °C
Richardson et al.[30]	LFP	-20 to 45	215 Hz	Z'	2-D SGM	Mean error = 0.6 °C

Beelen et al.[31]	Li-ion	-20 to 50	50 Hz	Z' & Z''	MC	RMS bias = 0.4 °C
Schmidt et al.[22]	NCA	-40 to 40	10.3 kHz	Z'	PF / LS	Error = 0.17 K
Zhang et al.[163]	LNO	-60 to 25	-	R _{ct} / R _{sei} / R _b	ECM	Unspecified
Srinivasan et al.[21]	LFP	-20 to 66	40 Hz	φ	None	Unspecified

Table 4. Comparison of studies that used impedance measurements to determine battery internal temperature; F₀ = intercept frequency; PF = polynomial fit; LS = least squares; MC = monte carlo; 2-D SGM = 2-D Spectral Galerkin Model; Z = impedance magnitude; TM = thermal model; DEKF = dual extended Kalman filter; DKF = dual Kalman filter; LC = linear correlation; NZIF = non zero intercept frequency.

8.3 State of Charge

Since the emergence of rechargeable batteries, attempts have been made to develop a system capable of estimating the available capacity. In recent years, much research has focused on improving the estimation of SOC, which is increasingly seen as the most important issue for EVs.[44, 202-204] The SOC of a battery is defined as the ratio of its current capacity (Q(t)) to the nominal capacity (Q_n).[205] The nominal capacity of a battery is the total amount of charge a battery can store.

$$SOC_{(t)} = \frac{Q_t}{Q_n} \quad (6)$$

SOC estimation can be regarded as the most important function of the BMS [43, 49, 79, 206] as it describes the current level of energy a LIB has, with the analogy of a 'fuel gauge' often being used. Accurate SOC estimates are fundamental in preventing the over-charging or discharging of LIBs, which can cause irreversible damage.[207, 208] Unfortunately, SOC is a parameter that cannot be directly measured. Batteries are nonlinear electrochemical systems that are affected by many consideration such as temperature, ageing and charge /

1
2
3 discharge cycles which makes SOC estimation complex and challenging to implement.[112,
4
5 209]

6
7 A precise SOC estimate is of particular importance for users of EVs, as it is vital they
8 know how much range is left and when a recharge needs to be performed.[140]
9 Environmental, behavioural and auxiliary (air-conditioning, lighting, windscreen wipers etc.)
10 factors need to be considered when predicting the available remaining capacity. [210, 211]
11 Lots of methods have been proposed to estimate SOC, given its indispensable nature, with CC
12 and OCV measurements being the two most common. In fact, it is not uncommon to have
13 combinations of two or more methods in conjunction with one another. [212] CC, also known
14 as ampere hour counting, is the simplest and most straightforward technique used to
15 estimate SOC. This method measures the current leaving the battery as a function of time to
16 estimate the current capacity. This value, and the previously estimated SOC value is used to
17 estimate the remaining capacity.[120]. The measurement of current is prone to errors and
18 noise. As a result, errors can accumulate over time causing a gradual decline in accuracy.
19 Furthermore, fluctuations in temperature and intensive cycling can influence SOC estimation.
20 Accuracy is highly dependent on the precision of the initial SOC estimate, which is not always
21 guaranteed. Drift and self-discharge can also become an issue after long periods of storage.
22 In spite of this, CC works well with LIBs because of their low self-discharge and leakage
23 current. [107, 120, 213, 214] Enhanced coulomb counters now account for ageing and
24 temperature based self-discharge but still require periodic calibration.
25
26
27
28
29
30
31
32
33
34
35
36
37
38
39

40
41 The OCV method is one of the most accurate for measuring SOC however, its
42 practicality in a BMS is limited as an extended time period at OCV is required.[215-217] When
43 measuring the OCV, it is understood that the battery must be disconnected from any load for
44 more than two hours as enough relaxation time is required to reach equilibrium.[218] For this
45 reason its practicality in a BMS is limited due to the long relaxation times required. The OCV-
46 SOC relationship differs between battery chemistries and changes with ageing and
47 temperature.[219-222]. Unlike lead-acid batteries, LIBs do not exhibit a straight-line
48 relationship between SOC and OCV.[44, 223]. This means a small error in OCV will amplify into
49 a large SOC error. To offset these shortcomings, the OCV method is usually used in
50 conjunction with another approach. For example, Mejdoubi et al. used an ECM and an EKF in
51 conjunction with battery OCV to estimate SOC.[224] Recent efforts have been made to reduce
52
53
54
55
56
57
58
59
60

1
2
3 the time required for cell relaxation, from a few hours to few minutes, significantly increasing
4 practical applications.[225, 226]. To deal with these problems, adaptive methods have been
5 applied with the CC or OCV approaches such as neural network (NN) [227, 228], FL [229],
6 adaptive observer [230, 231] and different variations of Kalman filters [79, 232-234]. A large
7 number of factors are necessary to develop and model a battery accurately which in turn
8 increases the computational burden on the BMS. Therefore, a trade-off between the
9 computational load and performance is often made when choosing a suitable SOC estimator.
10
11
12
13
14
15
16
17
18

19 8.3.1 State-of-Charge Estimation via Impedance

20
21 Battery impedance can be used for the recalibration for various battery states
22 including SOC.[235] As a battery cycles, impedance values can change significantly due to
23 external and internal factors. Internal factors include the batteries IT, SOH and SOC while
24 external factors include the environmental temperature, load or charge current and previous
25 usage of the battery.[6] Within specific frequency ranges, the dependence of one function
26 over another becomes negligible, thus allowing important information to be inferred.
27 Impedance has been used to estimate SOC in lead acid, NiMH, NiCd and LIB applications.[81,
28 235-238] This approach is like the OCV technique in that the SOC – OCV relationship is
29 substituted for an impedance – SOC relationship.[238] However, it is difficult to acquire an
30 independent SOC measurement as impedance is affected by other parameters.[11, 239]
31 Westerhoff *et al.* used two parameters acquired from EIS (R_{CT} and C_{DL}) and a simple ECM (Fig.
32 9a) comprised on only three circuit elements to estimate SOC [96] . SOC estimation accuracy
33 was found to be <5% in the middle range of SOC (30 % - 80 %) (Fig. 9b); however progressively
34 got worse as the SOC increased.
35
36
37
38
39
40
41
42
43
44
45
46
47
48
49
50
51
52
53
54
55
56
57
58
59
60

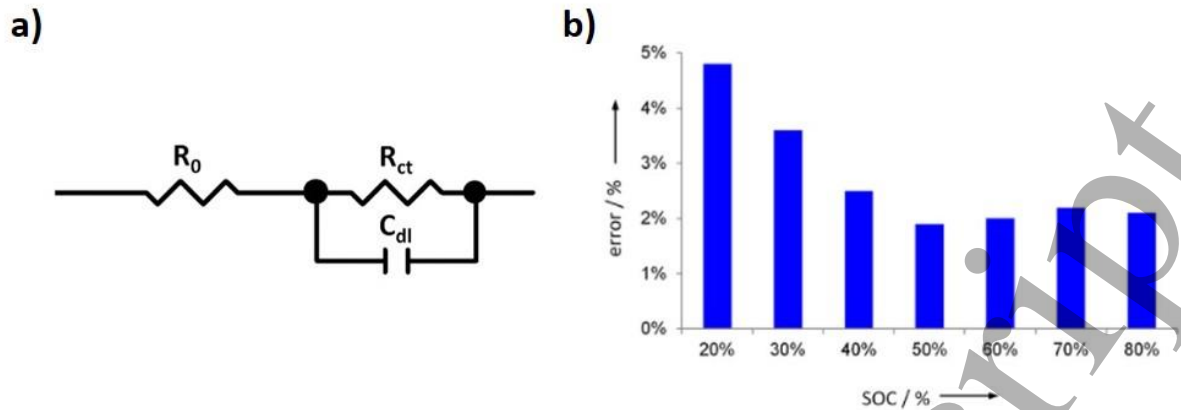


Fig. 9. a) Simple ECM comprised of three circuit elements. b) Maximum error of SOC estimate as a function of the SOC the estimate was performed.[96]¹³

Carkhuff *et al.* demonstrated a relationship between the real impedance at 2 Hz and SOC. At low frequencies, the battery impedance is SOC dependent and independent of SOH and temperature.[24] A similar low frequency impedance at two specific frequencies (0.32 Hz and 1.45 Hz) using geometric characteristics of the impedance spectrum was used by Lee and Choi to update the parameters of an ECM in combination with a least-squares fit to generate a SOC value.[240] Since it takes a long time to complete a full frequency EIS scan, this approach can shorten the time required dramatically (~ 70x) by examining just two frequencies and so is much more viable for commercial applications. Ran *et al.* substantiated the relationship between the maximum frequency of the semi-circle (f_{max}), the phase (ϕ) at 0.5 Hz and 1 Hz and the equivalent series capacitance (C_s) for predicting SOC with each showing a linear trend as a function of SOC. [241] Rodrigues *et al.* reported a similar relationship between SOC, f_{max} , C_s and the phase between 0.5 Hz to 5 Hz. [25] Cuadras & Kanoun found a relationship between Z_{mod} and SOC as well as the phase at 40 Hz demonstrating the large number of impedance parameters, both ECM components and specific frequencies, which have an intrinsic relationship with SOC.[242] Table 5 summarises existing studies that have used impedance for SOC estimation. At present, the majority of methods examined use impedance measurements to update an ECM. [95, 102, 243] For example, Wang, Howey, Osaka and Mingant all use ECMs as the basis of their models but use

¹³ Reprinted from Journal of Energy Storage, Vol. 8, U. Westerhoff, T. Kroker & K. Kurbach & M. Kurrat, Electrochemical impedance spectroscopy based estimation of the state of charge of lithium-ion batteries, Pages 244-256, Copyright (2016), with permission from Elsevier.

different methods to extract the SOC estimate e.g. least squares, particle filtering and Kalman filtering. [102-104, 243] Impedance data used to update an ECM can deliver SOC estimation accuracy's in the region of $> 1 - 5 \%$ error. If we compare this to a comprehensive review performed by Hannan et al., where the SOC estimation accuracy of a multitude of techniques was examined, we find that the average estimation error across 19 different techniques was 3.18 %.[44] Common techniques such as coulomb counting and the different forms of Kalman filter produced average estimation errors in the region of $< \pm 4 \%$ and $< \pm 1-4 \%$. Many learning and adaptive algorithms can achieve high estimation accuracy's but require large amounts of memory and are computationally heavy. EIS is advantageous as it is a low cost approach that can be easily implemented and can obtain SOC estimation accuracy's on par and better than other methods.

Author(s)	Battery Chemistry	Part of Impedance	f (Hz) for Model	Model	Accuracy
Lee & Choi[240]	LiPo	ECM updated using the Z' & Z'' at f 0.32 Hz & 1.45 Hz / TC	0.1 Hz – 1 kHz	ECM / LS / PF	Accuracy = 95.77 % - 99.15 %
Xu et al.[238]	NMC	ECM	0.3 Hz – 2.1 kHz	FOM /FKF / LS / GSM	Error = $\pm 1 \%$
Ran et al.[241]	LCO	$f_{\max} / \phi / C_s$	0.25 Hz – 100 kHz	ECM / LS	Unspecified
Cuadras & Kanoun [242]	LMD	ϕ at 40 Hz / Z_{mod}	40 Hz – 110 MHz	ECM	Unspecified
Osaka et al.[243]	LCO	ECM	0.1 Hz – 100 kHz	ECM	Depicted graphically
Howey et al.[102]	LFP / NMC	ECM	0.1 Hz – 10 kHz	ECM	Unspecified
Ma et al.[244]	LMO	ECM	-	ECM / FOM / FKF	Max. error = 0.5 %
Wang et al.[104]	LFP	ECM	0.1 Hz – 1kHz	ECM / PF / LOOCV	Unspecified

Rodrigues et al. [25]	LCO	f_{\max} / ϕ between 0.1 Hz – 5 Hz / $R_s /$ C_s	0.25 Hz – 100 kHz	ECM / LS	Unspecified
Pizarro – Carmona & Cortes-Carmona [245]	LFP	ECM	0.1 Hz – 1 kHz	ECM / ANN / GA / EKF	RMSRE = 1.19 %
Mu et al.[246]	NMC	ECM	-	ECM / FOM / GA / UKF	Error = 3 %
Chen et al.[247]	LFP	ECM	0.1 Hz – 10 kHz	ECM / FOM / HO	RMSE @25°C = 0.037 – 0.076 (dynamic test)
Westerhoff et al.[96]	NMC	$R_{ct} / C_{dl} / R_o$	0.1 Hz – 100 kHz	ECM / LS	Max. error = 5 %
Carkhuff et al.[24]	NCO	2 Hz	1 Hz – 1 kHz	-	-
Mingant et al.[103]	LFP	ECM	0.01 Hz – 100 kHz	ECM / LS / PF / LR	Error = 10 %

Table 5. Comparison of studies that have used AC impedance measurements to determine battery SOC; GA = generic algorithm; PS = particle swarm; FO = fractional order; UKF = unfiltered Kalman filter; HO = H-infinity observer; FKF = fractional Kalman filter; GSM = gain scheduling method; FOM = fractional order model; ECC = enhanced coulomb counter; PSO = particle swarm optimization; LOOCV = leave one out cross validation; C_2 = equivalent series capacitance; TC = time constants; Z_{mod} = impedance modulus.

9. Conclusion and Perspective

9.1 Summary

A review of existing studies that use impedance to access the SOC, SOH, IT and fault detection of LIBs has been performed. Detailed information regarding the model, battery chemistry, part of impedance, frequency and accuracy of each EIS estimation method has been listed and compared to existing estimation methods, which to the best of our knowledge is the most exhaustive review of the area to date. We have demonstrated that impedance

1
2
3 information can act as a useful input for a large variety of state estimation models. There are
4 a multitude of approaches and models in the field that range in complexity with a large
5 number of papers been published, particularly in recent years, on the topic. This review
6 summarises existing techniques with particular focus on the EIS metric and model used for
7 battery state estimation. The conclusions drawn are the following: (1) Impedance is
8 undoubtedly influenced by a combination of battery SOC, SOH and IT; (2) At certain
9 frequencies, the influence of one of these parameters is more sensitive than the others, thus,
10 allowing it to be estimated semi-independently of the others; (3) SOC estimation is dominated
11 by the use of ECMs, whose parameters are determined via impedance measurements,
12 whereas SOH and IT tend to use the correlation between impedance elements or specific
13 frequencies and themselves; (4) Studies estimating the same battery parameter or state often
14 use different impedance elements or frequency ranges demonstrating the lack of consensus
15 on the best approach for using impedance for battery state estimation; (6) The use of online
16 impedance in real-world applications has been proven viable; (7) The accuracy of EIS based
17 estimation techniques have been quantified and demonstrate comparable estimation
18 accuracies to estimating techniques. In summary, battery impedance has being shown to be
19 an effective tool for the estimation of SOH, SOC, IT and fault detection, however significant
20 issues still remain regarding its practical implementation in onboard applications. Recent
21 research has shown that incorporating and impedance device in onboard applications is
22 feasible. For EIS to be a part of a smart BMS, significant research still needs to be directed
23 towards its integration into existing battery systems. A BMS with onboard EIS will be able to
24 increase the sensing capabilities and state monitoring accuracy of an energy storage system.
25
26
27
28
29
30
31
32
33
34
35
36
37
38
39
40
41
42
43
44
45
46
47

9.2 Challenges

48
49
50 EIS has been shown to be a reliable laboratory based LIB characterisation tool but has
51 not yet proven its viability for integration in onboard BMSs. In light of this, the challenges
52 effecting its integration into real world applications must be evaluated. To further advance
53 the technology towards commercialization, we believe the principle challenge is the actual
54 embedding of an EIS capable device on existing BMSs. While we have discussed several
55 studies that have achieved this, for widespread adoption the cost per unit needs to be
56
57
58
59
60

1
2
3 reduced. This is particularly relevant for EVs, which contain hundreds of thousands of
4 interconnected batteries. Even a low cost is magnified dramatically when the large number
5 of cells is taken into account. Many researchers have used existing hardware in an EV to
6 measure impedance, which has the benefit of reducing the total cost of implementation.
7
8 Advanced switching technology between different modules could allow a single EIS device to
9 measure the impedance of multiple batteries but would introduce additional sources of noise.
10
11 With particular regard to power consumption, for small portable electronics, the level of
12 power required to run an EIS device is critical. Regardless of how much an EIS device could
13 improve state estimation, if the power consumption is too great it will not be commercially
14 viable. Furthermore, the size of such a device is important. In small compact devices such as
15 mobile phones, large amounts of additional space are not present. It is our opinion that
16 significant research already exists for estimating battery states using EIS and that the main
17 hurdle is now the practical implementation. The technical challenges of integrating EIS
18 hardware in onboard applications are vast. Reproducibility of accurate EIS measurements free
19 from noise on larger more complex battery systems has yet to be solved. In an EV,
20 interference from a myriad of external sources, varying environmental conditions, the
21 complex series and parallel networks of cells, and the constant changing state of the battery
22 make onboard EIS challenging to implement. Batteries for EVs have been trending to higher
23 capacities in recent years, with the consequence of having smaller impedances. An impedance
24 device must be sensitive enough to measure the response signal even when a DC bias,
25 multiple times larger than the response signal, is being used. Reducing these effects in an
26 optimal way is key to obtaining accurate EIS data. Most studies have been conducted in
27 laboratory settings. In order to make EIS state estimation a reality, more experimentation is
28 required to validate its use in real-world conditions.
29
30
31
32
33
34
35
36
37
38
39
40
41
42
43
44
45
46
47
48
49

50 **9.3 Outlook**

51
52 Perhaps the single greatest use for EIS in the coming years will be for the second-life
53 applications of EV batteries. Disposal of the battery pack adds additional costs, waste and
54 environmental damage to the batteries lifespan thus, many envisage a second-life for EV
55 batteries in less intensive applications such as in stationary energy storage. [248] The ability
56 to re-purpose a LIB in a second life application can have a large effect on the economics of
57
58
59
60

1
2
3 batteries. Feasibility studies have shown that for this to be economically viable, the whole
4 battery pack needs to be used without dismantling and inspecting each cell individually as this
5 will increase the time and cost required for evaluation.[249, 250] On-board EIS analysis could
6 provide the necessary information at a cell level to enable the entire pack to be used with the
7 benefit of leaving all contactors and connections in place, further reducing the cost.
8 Monitoring of individual cells using EIS throughout its entire lifespan could create a digital tag
9 providing accurate historical data, enabling a streamlined transition from one application to
10 another. The application of EIS for use in EVs requires additional research into the
11 modification of instrumentation and measurement to allow its implementation onto existing
12 BMSs. Notable work on the miniaturisation of EIS instrumentation exists, but are still many
13 years away from actual integration in an end-application. Several companies have made
14 significant advancements in developing a chip-scale EIS device. Panasonic recently announced
15 the development of a miniaturised EIS device that can accurately measure the impedance of
16 multiple interconnected cells.[251] Analog devices Inc. offer a commercial EIS device
17 (AD594X) designed specifically for battery applications. This device includes all necessary
18 hardware to create and measure impedances across a wide frequency range. [252]
19
20
21
22
23
24
25
26
27
28
29
30
31
32
33
34
35
36
37
38
39
40

41 **Acknowledgments**

42
43 This work was made possible by joint financial support from the Irish Research Council (IRC)
44 and Analog Devices International (ADI), under the IRC Enterprise Award Scheme (contract no.
45 EPSPG/2017/377).
46
47
48
49
50
51
52
53
54
55
56
57
58
59
60

References

- [1] X. Hu, C. Zou, C. Zhang, Y. Li, *IEEE Power and Energy Magazine*, 15 (2017) 20-31.
- [2] L. Lu, X. Han, J. Li, J. Hua, M. Ouyang, *J Power Sources*, 226 (2013) 272-288.
- [3] A. Opitz, P. Badami, L. Shen, K. Vignarooban, A.M. Kannan, *Renewable and Sustainable Energy Reviews*, 68 (2017) 685-692.
- [4] S.M. Rezvanianiani, Z. Liu, Y. Chen, J. Lee, *J Power Sources*, 256 (2014) 110-124.
- [5] Y. Xing, E.W. Ma, K.L. Tsui, M. Pecht, *Energies*, 4 (2011) 1840-1857.
- [6] A. Jossen, *J Power Sources*, 154 (2006) 530-538.
- [7] J. Remmlinger, M. Buchholz, M. Meiler, P. Bernreuter, K. Dietmayer, *J Power Sources*, 196 (2011) 5357-5363.
- [8] D.A. Howey, P.D. Mitcheson, V. Yufit, G.J. Offer, N.P. Brandon, *IEEE transactions on vehicular technology*, 63 (2013) 2557-2566.
- [9] R. Koch, R. Kuhn, I. Zilberman, A. Jossen, in: 2014 16th European Conference on Power Electronics and Applications, IEEE, 2014, pp. 1-10.
- [10] A. Zenati, P. Desprez, H. Razik, in: IECON 2010-36th Annual Conference on IEEE Industrial Electronics Society, IEEE, 2010, pp. 1773-1778.
- [11] W. Waag, S. Käbitz, D.U. Sauer, *Appl Energ*, 102 (2013) 885-897.
- [12] J. Zhu, Z. Sun, X. Wei, H. Dai, *J Power Sources*, 274 (2015) 990-1004.
- [13] R.J. Brodd, H.J. DeWane, *J Electrochem Soc*, 110 (1963) 1091-1097.
- [14] J.R. Macdonald, E. Barsoukov, *History*, 1 (2005) 1-13.
- [15] E. Karden, in, Verlag nicht ermittelbar, 2001.
- [16] N. Takami, A. Satoh, M. Hara, T. Ohsaki, *J Electrochem Soc*, 142 (1995) 371-379.
- [17] S.M. Lambert, M. Armstrong, P.S. Attidekou, P.A. Christensen, J.D. Widmer, C. Wang, K. Scott, *IEEE Transactions on Industrial Electronics*, 64 (2016) 4017-4026.
- [18] J. Huber, C. Tammer, D. Schneider, C. Seidel, G. Reinhart, *Procedia CIRP*, 62 (2017) 423-428.
- [19] E. Karden, S. Buller, R.W. De Doncker, *Electrochimica Acta*, 47 (2002) 2347-2356.
- [20] F. Huet, *J Power Sources*, 70 (1998) 59-69.
- [21] R. Srinivasan, B.G. Carkhuff, M.H. Butler, A.C. Baisden, *Electrochim Acta*, 56 (2011) 6198-6204.
- [22] J.P. Schmidt, S. Arnold, A. Loges, D. Werner, T. Wetzels, E. Ivers-Tiffée, *J Power Sources*, 243 (2013) 110-117.
- [23] D.I. Stroe, M. Swierczynski, A.I. Stan, V. Knap, R. Teodorescu, S.J. Andreasen, in: 2014 IEEE Energy Conversion Congress and Exposition (ECCE), IEEE, 2014, pp. 4576-4582.
- [24] B.G. Carkhuff, P.A. Demirev, R. Srinivasan, *IEEE Transactions on Industrial Electronics*, 65 (2018) 6497-6504.
- [25] S. Rodrigues, N. Munichandraiah, A. Shukla, *J Solid State Electr*, 3 (1999) 397-405.
- [26] M. Galeotti, L. Cinà, C. Giammanco, S. Cordiner, A. Di Carlo, *Energy*, 89 (2015) 678-686.
- [27] X. Zhou, Z. Pan, X. Han, L. Lu, M. Ouyang, *J Power Sources*, 417 (2019) 188-192.
- [28] Y. Zhang, Q. Tang, Y. Zhang, J. Wang, U. Stimming, A.A. Lee, *Nat Commun*, 11 (2020) 1-6.
- [29] L. Raijmakers, D. Danilov, J. Van Lammeren, M. Lammers, P. Notten, *J Power Sources*, 247 (2014) 539-544.
- [30] R.R. Richardson, P.T. Ireland, D.A. Howey, *J Power Sources*, 265 (2014) 254-261.
- [31] H. Beelen, L. Raijmakers, M. Donkers, P. Notten, H. Bergveld, *IFAC-PapersOnLine*, 48 (2015) 383-388.
- [32] H. Beelen, L. Raijmakers, M. Donkers, P. Notten, H. Bergveld, *Appl Energ*, 175 (2016) 128-140.
- [33] W. Huang, J.A.A. Qahouq, *IEEE Transactions on Industrial Electronics*, 61 (2014) 5987-5995.
- [34] E. Din, C. Schaef, K. Moffat, J.T. Stauth, *IEEE Transactions on Power Electronics*, 32 (2016) 5688-5698.
- [35] Z. Gong, Z. Liu, Y. Wang, K. Gupta, C. Da Silva, T. Liu, Z. Zheng, W. Zhang, J.M. van Lammeren, H. Bergveld, in: 2018 IEEE Applied Power Electronics Conference and Exposition (APEC), IEEE, 2018, pp. 1922-1929.

- 1
2
3 [36] M.A. Varnosfaderani, D. Strickland, in: 2016 18th European Conference on Power Electronics
4 and Applications (EPE'16 ECCE Europe), IEEE, 2016, pp. 1-10.
5 [37] Z. Xia, J.A.A. Qahouq, in: 2017 IEEE Applied Power Electronics Conference and Exposition
6 (APEC), IEEE, 2017, pp. 1999-2003.
7 [38] C. Campestrini, M.F. Horsche, I. Zilberman, T. Heil, T. Zimmermann, A. Jossen, *J Energy Storage*,
8 7 (2016) 38-51.
9 [39] Z. Chen, B. Xia, C. You, C.C. Mi, *Applied Energy*, 145 (2015) 172-179.
10 [40] P. Zhou, Z. He, T. Han, X. Li, X. Lai, L. Yan, T. Lv, J. Xie, Y. Zheng, *Energy Reports*, 6 (2020) 672-
11 683.
12 [41] W. Waag, C. Fleischer, D.U. Sauer, *J Power Sources*, 258 (2014) 321-339.
13 [42] A. Barré, B. Deguilhem, S. Grolleau, M. Gérard, F. Suard, D. Riu, *J Power Sources*, 241 (2013)
14 680-689.
15 [43] V. Agarwal, K. Uthaichana, R.A. DeCarlo, L.H. Tsoukalas, *IEEE Transactions on Energy Conversion*,
16 25 (2010) 821-835.
17 [44] M.A. Hannan, M.H. Lipu, A. Hussain, A. Mohamed, *Renewable and Sustainable Energy Reviews*,
18 78 (2017) 834-854.
19 [45] L. Ungurean, G. Cârstoiu, M.V. Micea, V. Groza, *International Journal of Energy Research*, 41
20 (2017) 151-181.
21 [46] H. Liu, Z. Wei, W. He, J. Zhao, *Energy conversion and management*, 150 (2017) 304-330.
22 [47] G. Xia, L. Cao, G. Bi, *J Power Sources*, 367 (2017) 90-105.
23 [48] H. Rahimi-Eichi, U. Ojha, F. Baronti, M.-Y. Chow, *IEEE Industrial Electronics Magazine*, 7 (2013) 4-
24 16.
25 [49] K.W.E. Cheng, B. Divakar, H. Wu, K. Ding, H.F. Ho, *IEEE transactions on vehicular technology*, 60
26 (2010) 76-88.
27 [50] S. Zhang, K. Xu, T. Jow, *Electrochemistry communications*, 4 (2002) 928-932.
28 [51] D.H. Doughty, E.P. Roth, *The Electrochemical Society Interface*, 21 (2012) 37.
29 [52] D.H. Doughty, E.P. Roth, *Electrochemical Society Interface*, 21 (2012) 37.
30 [53] G. Pérez, M. Garmendia, J.F. Reynaud, J. Crego, U. Viscarret, *Appl Energ*, 155 (2015) 834-845.
31 [54] C. Gabrielli, Identification of electrochemical processes by frequency response analysis:
32 technical report number 004/83, Schlumberger Instruments, 1984.
33 [55] N. Hampson, S. Karunathilaka, R. Leek, *Journal of Applied Electrochemistry*, 10 (1980) 3-11.
34 [56] P. Křivík, S. Vaculík, P. Bača, J. Kazelle, *J Energy Storage*, 21 (2019) 581-585.
35 [57] T.B. Reddy, *Linden's handbook of batteries*, Mcgraw-hill New York, 2011.
36 [58] M.V. Reddy, G.V. Subba Rao, B.V.R. Chowdari, *The Journal of Physical Chemistry C*, 111 (2007)
37 11712-11720.
38 [59] A. Hammouche, E. Karden, R.W. De Doncker, *J Power Sources*, 127 (2004) 105-111.
39 [60] Y. Xie, J. Li, C. Yuan, *Electrochim Acta*, 127 (2014) 266-275.
40 [61] M.E. Orazem, B. Tribollet, *Electrochemical impedance spectroscopy*, John Wiley & Sons, 2017.
41 [62] P.A. Lindahl, M.A. Cornachione, S.R. Shaw, *IEEE Transactions on Instrumentation and*
42 *Measurement*, 61 (2012) 3303-3311.
43 [63] D. Andre, M. Meiler, K. Steiner, C. Wimmer, T. Soczka-Guth, D. Sauer, *J Power Sources*, 196
44 (2011) 5334-5341.
45 [64] D. Bell, *Fundamentals of Electric Circuits*, Oxford University Press, 2009.
46 [65] P. Verma, P. Maire, P. Novák, *Electrochim Acta*, 55 (2010) 6332-6341.
47 [66] Y. Susumu, N. Koichi, *Electrical Engineering in Japan*, 180 (2012) 29-37.
48 [67] M.-T. von Srbik, M. Marinescu, R.F. Martinez-Botas, G.J. Offer, *J Power Sources*, 325 (2016) 171-
49 184.
50 [68] X. Zhang, W. Zhang, G. Lei, *Trans. Electr. Electron. Mater.(TEEM)*, 17 (2016) 311-316.
51 [69] X. Zhang, J. Lu, S. Yuan, J. Yang, X. Zhou, *J Power Sources*, 345 (2017) 21-29.
52 [70] E. Ferg, C. Rossouw, P. Loyson, *J Power Sources*, 226 (2013) 299-305.
53
54
55
56
57
58
59
60

- [71] H.-G. Schweiger, O. Obeidi, O. Komesker, A. Raschke, M. Schiemann, C. Zehner, M. Gehnen, M. Keller, P. Birke, *Sensors*, 10 (2010) 5604-5625.
- [72] F. Joho, P. Novák, M.E. Spahr, *J Electrochem Soc*, 149 (2002) A1020-A1024.
- [73] H. Jannesari, M. Emami, C. Ziegler, *J Power Sources*, 196 (2011) 9654-9664.
- [74] P. Arora, R.E. White, M. Doyle, *J Electrochem Soc*, 145 (1998) 3647-3667.
- [75] O. Erdinc, B. Vural, M. Uzunoglu, in: 2009 International Conference on Clean Electrical Power, IEEE, 2009, pp. 383-386.
- [76] T. Tuan, V.-L. Tran, W. Choi, Development of the intelligent charger with battery State-Of-Health estimation using online impedance spectroscopy, 2014.
- [77] D.A. Howey, P.D. Mitcheson, V. Yufit, G.J. Offer, N.P. Brandon, *IEEE Transactions on Vehicular Technology*, 63 (2014) 2557-2566.
- [78] N. Thanh-Tuan, T. Van-Long, C. Woojin, in: Proc IEEE Int Symp, 2014, pp. 454-458.
- [79] H. Dai, X. Wei, Z. Sun, J. Wang, W. Gu, *Appl Energ*, 95 (2012) 227-237.
- [80] J.D. Kozlowski, in: 2003 IEEE Aerospace Conference Proceedings (Cat. No. 03TH8652), IEEE, 2003, pp. 3257-3270.
- [81] A.H. Ranjbar, A. Banaei, A. Khoobroo, B. Fahimi, *IEEE Transactions on Smart Grid*, 3 (2011) 360-367.
- [82] Z. Xia, J.A.A. Qahouq, in: 2019 IEEE Applied Power Electronics Conference and Exposition (APEC), IEEE, 2019, pp. 3361-3365.
- [83] M.E. Orazem, B. Tribollet, New Jersey, (2008) 383-389.
- [84] M. Kassem, J. Bernard, R. Revel, S. Pelissier, F. Duclaud, C. Delacourt, *J Power Sources*, 208 (2012) 296-305.
- [85] C.T. Love, K. Swider-Lyons, *Electrochemical and Solid-State Letters*, 15 (2012) A53-A56.
- [86] S. Moore, P. Barendse, in: *IEEE Ener Conv*, IEEE, 2017, pp. 5617-5624.
- [87] J.E.B. Randles, *Discussions of the faraday society*, 1 (1947) 11-19.
- [88] M. Levi, D. Aurbach, *The Journal of Physical Chemistry B*, 108 (2004) 11693-11703.
- [89] U. Tröltzsch, O. Kanoun, H.-R. Tränkler, *Electrochim Acta*, 51 (2006) 1664-1672.
- [90] Y. Zhang, C.-Y. Wang, *J Electrochem Soc*, 156 (2009) A527-A535.
- [91] C. Pastor-Fernández, K. Uddin, G.H. Chouchelamane, W.D. Widanage, J. Marco, *J Power Sources*, 360 (2017) 301-318.
- [92] Q.-A. Huang, Y. Shen, Y. Huang, L. Zhang, J. Zhang, *Electrochim Acta*, 219 (2016) 751-765.
- [93] K. Bundy, M. Karlsson, G. Lindbergh, A. Lundqvist, *J Power Sources*, 72 (1998) 118-125.
- [94] H. Jing, Y. Huimei, in: 2015 IEEE 10th Conference on Industrial Electronics and Applications (ICIEA), 2015, pp. 794-799.
- [95] R. Mingant, J. Bernard, V. Sauvart-Moynot, A. Delaille, S. Mailley, J.L. Hognon, F. Huet, in: *ECS Transactions*, 2011, pp. 41-53.
- [96] U. Westerhoff, T. Kroker, K. Kurbach, M. Kurrat, *J Energy Storage*, 8 (2016) 244-256.
- [97] G.L. Plett, *J Power Sources*, 134 (2004) 252-261.
- [98] H. He, R. Xiong, X. Zhang, F. Sun, J. Fan, *IEEE Transactions on Vehicular Technology*, 60 (2011) 1461-1469.
- [99] J. Huang, Z. Li, B.Y. Liaw, J. Zhang, *J Power Sources*, 309 (2016) 82-98.
- [100] J.R. Macdonald, *Journal of Physics: Condensed Matter*, 24 (2012) 175004.
- [101] A. Eddahech, O. Briat, E. Woïrgard, J.-M. Vinassa, *Microelectronics Reliability*, 52 (2012) 2438-2442.
- [102] D. Howey, V. Yufit, P. Mitcheson, G. Offer, N. Brandon, in: 2013 World Electric Vehicle Symposium and Exhibition (EVS27), IEEE, 2013, pp. 1-7.
- [103] R. Mingant, J. Bernard, V.S. Moynot, A. Delaille, S. Mailley, J.-L. Hognon, F. Huet, *ECS Transactions*, 33 (2011) 41.
- [104] Q.-K. Wang, Y.-J. He, J.-N. Shen, X.-S. Hu, Z.-F. Ma, *IEEE Transactions on Power Electronics*, 33 (2017) 8449-8460.
- [105] X. Wei, X. Wang, H. Dai, *Energies*, 11 (2018) 64.

- [106] B. Rosca, J.T.B.A. Kessels, H.J. Bergveld, P.P.J.v.d. Bosch, in: 2012 IEEE Vehicle Power and Propulsion Conference, 2012, pp. 1122-1127.
- [107] S. Piller, M. Perrin, A. Jossen, *J Power Sources*, 96 (2001) 113-120.
- [108] D. Le, X. Tang, in: Annual conference of the prognostics and health management society, 2011, pp. 367-373.
- [109] K. Goebel, B. Saha, A. Saxena, J.R. Celaya, J.P. Christophersen, *IEEE instrumentation & measurement magazine*, 11 (2008) 33-40.
- [110] D. Andre, A. Nuhic, T. Soczka-Guth, D.U. Sauer, *Engineering Applications of Artificial Intelligence*, 26 (2013) 951-961.
- [111] M. Daboussy, D. Chrenko, E.-H. Aglzim, Z.H.C. Daud, L. Le Moyne, in: 2013 IEEE Transportation Electrification Conference and Expo (ITEC), IEEE, 2013, pp. 1-6.
- [112] N. Watrin, B. Blunier, A. Miraoui, in: 2012 IEEE Transportation Electrification Conference and Expo (ITEC), IEEE, 2012, pp. 1-6.
- [113] J. Vetter, P. Novák, M.R. Wagner, C. Veit, K.-C. Möller, J. Besenhard, M. Winter, M. Wohlfahrt-Mehrens, C. Vogler, A. Hammouche, *J Power Sources*, 147 (2005) 269-281.
- [114] X. Hu, S.E. Li, Z. Jia, B. Egardt, *Energy*, 64 (2014) 953-960.
- [115] M. Broussely, P. Biensan, F. Bonhomme, P. Blanchard, S. Herreyre, K. Nechev, R. Staniewicz, *J Power Sources*, 146 (2005) 90-96.
- [116] S.B. Peterson, J. Apt, J. Whitacre, *J Power Sources*, 195 (2010) 2385-2392.
- [117] W. van Schalkwijk, B. Scrosati, in: Plenum, New York, 2002.
- [118] B.Y. Liaw, R.G. Jungst, G. Nagasubramanian, H.L. Case, D.H. Doughty, *Journal of power sources*, 140 (2005) 157-161.
- [119] C.R. Birkel, M.R. Roberts, E. McTurk, P.G. Bruce, D.A. Howey, *J Power Sources*, 341 (2017) 373-386.
- [120] K.S. Ng, C.-S. Moo, Y.-P. Chen, Y.-C. Hsieh, *Appl Energ*, 86 (2009) 1506-1511.
- [121] M.S. El Din, M.F. Abdel-Hafez, A.A. Hussein, *IEEE Transactions on Vehicular Technology*, 65 (2015) 4608-4618.
- [122] B. Pattipati, C. Sankavaram, K. Pattipati, *IEEE Transactions on Systems, Man, and Cybernetics, Part C (Applications and Reviews)*, 41 (2011) 869-884.
- [123] M. Daboussy, D. Chrenko, E.H. Aglzim, Z.H.C. Daud, L.L. Moyne, in: 2013 IEEE Transportation Electrification Conference and Expo (ITEC), 2013, pp. 1-6.
- [124] A. Eddahech, M. Ayadi, O. Briat, J.-M. Vinassa, in: 4th International Conference on Power Engineering, Energy and Electrical Drives, IEEE, 2013, pp. 1460-1465.
- [125] D. Andre, C. Appel, T. Soczka-Guth, D.U. Sauer, *J Power Sources*, 224 (2013) 20-27.
- [126] E.A. Wan, R.V.D. Merwe, in: Proceedings of the IEEE 2000 Adaptive Systems for Signal Processing, Communications, and Control Symposium (Cat. No.00EX373), 2000, pp. 153-158.
- [127] A.J. Salkind, C. Fennie, P. Singh, T. Atwater, D.E. Reisner, *J Power Sources*, 80 (1999) 293-300.
- [128] P. Singh, C. Fennie, D. Reisner, *J Power Sources*, 136 (2004) 322-333.
- [129] M. Shahriari, M. Farrokhi, *IEEE Transactions on Industrial Electronics*, 60 (2012) 191-202.
- [130] A. Eddahech, O. Briat, N. Bertrand, J.-Y. Deletage, J.-M. Vinassa, *International Journal of Electrical Power & Energy Systems*, 42 (2012) 487-494.
- [131] X. Wang, X. Wei, H. Dai, *J Energy Storage*, 21 (2019) 618-631.
- [132] H.-F. Yuan, L.-R. Dung, *IEEE Transactions on Vehicular Technology*, 66 (2016) 2019-2032.
- [133] L. Chen, Z. Lü, W. Lin, J. Li, H. Pan, *Measurement*, 116 (2018) 586-595.
- [134] J. Jiang, Z. Lin, Q. Ju, Z. Ma, C. Zheng, Z. Wang, *Energy Procedia*, 105 (2017) 844-849.
- [135] P. Singh, S. Kaneria, J. Broadhead, X. Wang, J. Burdick, in: INTELEC 2004. 26th Annual International Telecommunications Energy Conference, 2004, pp. 524-531.
- [136] C.T. Love, M.B. Virji, R.E. Rocheleau, K.E. Swider-Lyons, *Journal of Power Sources*, 266 (2014) 512-519.
- [137] M. Berecibar, I. Gandiaga, I. Villarreal, N. Omar, J. Van Mierlo, P. Van den Bossche, *Renewable and Sustainable Energy Reviews*, 56 (2016) 572-587.

- [138] W. Haiying, H. Long, S. Jianhua, L. Shuanquan, W. Feng, in: Proceedings of 2011 6th International Forum on Strategic Technology, IEEE, 2011, pp. 261-264.
- [139] A. Zenati, P. Desprez, H. Razik, in: IECON 2010 - 36th Annual Conference on IEEE Industrial Electronics Society, 2010, pp. 1773-1778.
- [140] X. Wang, X. Wei, H. Dai, Q. Wu, in: 2015 IEEE Vehicle Power and Propulsion Conference (VPPC), IEEE, 2015, pp. 1-5.
- [141] E.A. Olivetti, G. Ceder, G.G. Gaustad, X. Fu, *Joule*, 1 (2017) 229-243.
- [142] C. Hendricks, N. Williard, S. Mathew, M. Pecht, *J Power Sources*, 297 (2015) 113-120.
- [143] Q. Wang, B. Mao, S.I. Stoliarov, J. Sun, *Progress in Energy and Combustion Science*, 73 (2019) 95-131.
- [144] P.A. Wicaksono, R.F. Jasmine, M. Rifni, D.P. Sirait, R.F.J. Sakti, *Advances in Transportation and Logistics Research*, 1 (2018) 1160-1169.
- [145] S. Socher, C. Jehle, U. Potthoff, *Transportation Research Procedia*, 14 (2016) 3661-3666.
- [146] D. Mukoyama, T. Momma, H. Nara, T. Osaka, *Chemistry Letters*, 41 (2012) 444-446.
- [147] T.C. Kaypmaz, R.N. Tuncay, in: 2011 IEEE Vehicle Power and Propulsion Conference, IEEE, 2011, pp. 1-5.
- [148] A. Singh, A. Izadian, S. Anwar, in: IECON 2013-39th Annual Conference of the IEEE Industrial Electronics Society, IEEE, 2013, pp. 3524-3529.
- [149] C.T. Love, K. Swider-Lyons, *Electrochemical and Solid State Letters*, 15 (2012) A53.
- [150] N.S. Spinner, C.T. Love, S.L. Rose-Pehrsson, S.G. Tuttle, *Electrochim Acta*, 174 (2015) 488-493.
- [151] G.-H. Kim, K. Smith, J. Ireland, A. Pesaran, *J Power Sources*, 210 (2012) 243-253.
- [152] G. Lacey, T. Jiang, G. Putrus, R. Kotter, in: 2013 48th International Universities' Power Engineering Conference (UPEC), IEEE, 2013, pp. 1-7.
- [153] Z. An, L. Jia, Y. Ding, C. Dang, X. Li, *Journal of Thermal Science*, 26 (2017) 391-412.
- [154] N.S. Spinner, C.R. Field, M.H. Hammond, B.A. Williams, K.M. Myers, A.L. Lubrano, S.L. Rose-Pehrsson, S.G. Tuttle, *J Power Sources*, 279 (2015) 713-721.
- [155] T.M. Bandhauer, S. Garimella, T.F. Fuller, *J Electrochem Soc*, 158 (2011) R1-R25.
- [156] F. Larsson, B.-E. Mellander, *J Electrochem Soc*, 161 (2014) A1611.
- [157] P. Balakrishnan, R. Ramesh, T.P. Kumar, *J Power Sources*, 155 (2006) 401-414.
- [158] O. Haik, S. Ganin, G. Gershinsky, E. Zinigrad, B. Markovsky, D. Aurbach, I. Halalay, *J Electrochem Soc*, 158 (2011) A913-A923.
- [159] Q. Wang, J. Sun, X. Yao, C. Chen, *J Electrochem Soc*, 153 (2006) A329-A333.
- [160] C.G. Motloch, J.P. Christophersen, J.R. Belt, R.B. Wright, G.L. Hunt, R.A. Sutula, T. Duong, T.J. Tartamella, H.J. Haskins, T.J. Miller, *SAE Transactions*, (2002) 797-802.
- [161] S. Tippmann, D. Walper, L. Balboa, B. Spier, W.G. Bessler, *J Power Sources*, 252 (2014) 305-316.
- [162] G. Zhang, L. Cao, S. Ge, C.-Y. Wang, C.E. Shaffer, C.D. Rahn, *J Electrochem Soc*, 161 (2014) A1499-A1507.
- [163] S. Zhang, K. Xu, T. Jow, *Electrochim Acta*, 49 (2004) 1057-1061.
- [164] G. Nagasubramanian, *Journal of applied electrochemistry*, 31 (2001) 99-104.
- [165] X. Lin, H.E. Perez, J.B. Siegel, A.G. Stefanopoulou, Y. Li, R.D. Anderson, Y. Ding, M.P. Castanier, *IEEE Transactions on Control Systems Technology*, 21 (2012) 1745-1755.
- [166] W. Wu, X. Xiao, X. Huang, *Electrochim Acta*, 83 (2012) 227-240.
- [167] R.R. Richardson, S. Zhao, D.A. Howey, *J Power Sources*, 327 (2016) 726-735.
- [168] S. Santhanagopalan, P. Ramadass, J.Z. Zhang, *Journal of Power Sources*, 194 (2009) 550-557.
- [169] A.A. Pesaran, G.-H. Kim, M. Keyser, in: National Renewable Energy Lab.(NREL), Golden, CO (United States), 2009.
- [170] X. Lin, A.G. Stefanopoulou, J.B. Siegel, S. Mohan, in: ASME 2014 Dynamic Systems and Control Conference, American Society of Mechanical Engineers Digital Collection, 2014.
- [171] G.-H. Kim, A. Pesaran, R. Spotnitz, *J Power Sources*, 170 (2007) 476-489.
- [172] G. Guo, B. Long, B. Cheng, S. Zhou, P. Xu, B. Cao, *J Power Sources*, 195 (2010) 2393-2398.
- [173] H. Sun, X. Wang, B. Tossan, R. Dixon, *J Power Sources*, 206 (2012) 349-356.

- 1
2
3 [174] C. Zhang, K. Li, J. Deng, *J Power Sources*, 302 (2016) 146-154.
4 [175] Z. Li, J. Zhang, B. Wu, J. Huang, Z. Nie, Y. Sun, F. An, N. Wu, *J Power Sources*, 241 (2013) 536-
5 553.
6 [176] M.S.K. Mutyala, J. Zhao, J. Li, H. Pan, C. Yuan, X. Li, *J Power Sources*, 260 (2014) 43-49.
7 [177] V. Srinivasan, C.Y. Wang, *J Electrochem Soc*, 150 (2003) A98-A106.
8 [178] W. Gu, C. Wang, *J Electrochem Soc*, 147 (2000) 2910.
9 [179] F. Baronti, *Proc. IEEE Int. Conf. Appl. Electron.*, (2011) 1-5.
10 [180] M.-H. Chang, H.-P. Huang, S.-W. Chang, *Energies*, 6 (2013) 2007-2030.
11 [181] E. Barsoukov, J.R. Macdonald, *Applications*, 2nd ed.(Hoboken, NJ: John Wiley & Sons, Inc.,
12 2005), (2005).
13 [182] R. Koch, A. Jossen, in: *EVS28 International Electric Vehicle Symposium and Exhibition*, 2015,
14 pp. 1-9.
15 [183] H. Beelen, K. Mundaragi Shivakumar, L. Raijmakers, M. Donkers, H.J. Bergveld, *International*
16 *Journal of Energy Research*, 44 (2020) 2889-2908.
17 [184] R. Srinivasan, *J Power Sources*, 198 (2012) 351-358.
18 [185] R. Srinivasan, B.G. Carkhuff, *J Power Sources*, 241 (2013) 560-566.
19 [186] J.P. Schmidt, D. Manka, D. Klotz, E. Ivers-Tiffée, *J Power Sources*, 196 (2011) 8140-8146.
20 [187] J.P. Schmidt, T. Chrobak, M. Ender, J. Illig, D. Klotz, E. Ivers-Tiffée, *J Power Sources*, 196 (2011)
21 5342-5348.
22 [188] X. Lin, H.E. Perez, S. Mohan, J.B. Siegel, A.G. Stefanopoulou, Y. Ding, M.P. Castanier, *J Power*
23 *Sources*, 257 (2014) 1-11.
24 [189] P. Suresh, A. Shukla, N. Munichandraiah, *Journal of applied electrochemistry*, 32 (2002) 267-
25 273.
26 [190] E. Barsoukov, J.H. Jang, H. Lee, *J Power Sources*, 109 (2002) 313-320.
27 [191] M. Thomas, P. Bruce, J.B. Goodenough, *J Electrochem Soc*, 132 (1985) 1521.
28 [192] D. Abraham, E. Reynolds, E. Sammann, A. Jansen, D. Dees, *Electrochimica Acta*, 51 (2005) 502-
29 510.
30 [193] T. Stanciu, D.-I. Stroe, R. Teodorescu, M. Swierczynski, in: *Eur Conf Pow Electr, IEEE*, 2015, pp.
31 1-10.
32 [194] Y. Troxler, B. Wu, M. Marinescu, V. Yufit, Y. Patel, A.J. Marquis, N.P. Brandon, G.J. Offer, *J*
33 *Power Sources*, 247 (2014) 1018-1025.
34 [195] R. Richardson, in, *University of Oxford*, 2016.
35 [196] L.H.J. Raijmakers, D.L. Danilov, J.P.M.v. Lammeren, T.J.G. Lammers, H.J. Bergveld, P.H.L.
36 Notten, *IEEE Transactions on Industrial Electronics*, 63 (2016) 3168-3178.
37 [197] B. Shabani, M. Biju, *Energies*, 8 (2015) 10153-10177.
38 [198] R.R. Richardson, D.A. Howey, *IEEE Transactions on Sustainable Energy*, 6 (2015) 1190-1199.
39 [199] P. Haussmann, J. Melbert, *SAE International Journal of Alternative Powertrains*, 6 (2017).
40 [200] L.H. Raijmakers, D.L. Danilov, J.P. Van Lammeren, T.J. Lammers, H.J. Bergveld, P.H. Notten, *IEEE*
41 *Transactions on Industrial Electronics*, 63 (2016) 3168-3178.
42 [201] J.-q. Li, L. Fang, W. Shi, X. Jin, *Energy*, 148 (2018) 247-257.
43 [202] K. Young, C. Wang, K. Strunz, *Electric vehicle battery technologies*, in: *Electric vehicle*
44 *integration into modern power networks*, Springer, 2013, pp. 15-56.
45 [203] H. Banvait, S. Anwar, Y. Chen, in: *2009 American control conference, IEEE*, 2009, pp. 3938-
46 3943.
47 [204] I.-S. Kim, *IEEE Transactions on Power Electronics*, 23 (2008) 2027-2034.
48 [205] W.-Y. Chang, *ISRN Applied Mathematics*, 2013 (2013).
49 [206] L. Maharjan, S. Inoue, H. Akagi, J. Asakura, *IEEE Transactions on Power Electronics*, 24 (2009)
50 1628-1636.
51 [207] H. He, R. Xiong, H. Guo, *Appl Energ*, 89 (2012) 413-420.
52 [208] Y. Wang, H. Fang, Z. Sahinoglu, T. Wada, S. Hara, *IEEE Transactions on Control Systems*
53 *Technology*, 23 (2014) 948-962.
54
55
56
57
58
59
60

- 1
2
3 [209] X. Hu, R. Xiong, B. Egardt, IEEE Transactions on Industrial Informatics, 10 (2013) 1948-1959.
4 [210] K. Sarrafan, D. Sutanto, K.M. Muttaqi, G. Town, IET Electrical Systems in Transportation, 7
5 (2016) 117-124.
6 [211] O. Kanoun, Progress Reports on Impedance Spectroscopy: Measurements, Modeling, and
7 Application, Walter de Gruyter GmbH & Co KG, 2016.
8 [212] C. Fleischer, W. Waag, Z. Bai, D.U. Sauer, Journal of Power Electronics, 13 (2013) 516-527.
9 [213] J. Alzieu, H. Smimite, C. Glaize, J Power Sources, 67 (1997) 157-161.
10 [214] Y. Zheng, M. Ouyang, X. Han, L. Lu, J. Li, J Power Sources, 377 (2018) 161-188.
11 [215] S. Lee, J. Kim, J. Lee, B.H. Cho, J Power Sources, 185 (2008) 1367-1373.
12 [216] Y. Xing, W. He, M. Pecht, K.L. Tsui, Appl Energ, 113 (2014) 106-115.
13 [217] B. Pattipati, B. Balasingam, G. Avvari, K. Pattipati, Y. Bar-Shalom, J Power Sources, 269 (2014)
14 317-333.
15 [218] F. Yang, W. Li, C. Li, Q. Miao, Energy, 175 (2019) 66-75.
16 [219] M.W. Cheng, Y.S. Lee, M. Liu, C.C. Sun, IET Electrical Systems in Transportation, 5 (2015) 70-76.
17 [220] L. Lavigne, J. Sabatier, J.M. Francisco, F. Guillemard, A. Noury, J Power Sources, 324 (2016) 694-
18 703.
19 [221] S. Tong, M.P. Klein, J.W. Park, J Power Sources, 293 (2015) 416-428.
20 [222] A. Manthopoulos, X. Wang, in: IECON 2020 The 46th Annual Conference of the IEEE Industrial
21 Electronics Society, IEEE, 2020, pp. 2385-2392.
22 [223] M. Coleman, C.K. Lee, C. Zhu, W.G. Hurley, IEEE Transactions on Industrial Electronics, 54
23 (2007) 2550-2557.
24 [224] A.E. Mejdoubi, A. Oukaour, H. Chaoui, H. Gualous, J. Sabor, Y. Slamani, IEEE Transactions on
25 Industrial Electronics, 63 (2016) 2391-2402.
26 [225] W. Waag, D.U. Sauer, Appl Energ, 111 (2013) 416-427.
27 [226] J. Groenewald, T. Grandjean, J. Marco, Renewable and Sustainable Energy Reviews, 69 (2017)
28 98-111.
29 [227] W. He, N. Williard, C. Chen, M. Pecht, International Journal of Electrical Power & Energy
30 Systems, 62 (2014) 783-791.
31 [228] T. Parthiban, R. Ravi, N. Kalaiselvi, Electrochim Acta, 53 (2007) 1877-1882.
32 [229] A.J. Salkind, C. Fennie, P. Singh, T. Atwater, D.E. Reisner, J Power Sources, 80 (1999) 293-300.
33 [230] X. Hu, F. Sun, Y. Zou, Energies, 3 (2010) 1586-1603.
34 [231] F. Zhong, H. Li, S. Zhong, Q. Zhong, C. Yin, Communications in Nonlinear Science and Numerical
35 Simulation, 24 (2015) 127-144.
36 [232] J. Lee, O. Nam, B. Cho, J Power Sources, 174 (2007) 9-15.
37 [233] G.L. Plett, J Power Sources, 161 (2006) 1369-1384.
38 [234] G.L. Plett, J Power Sources, 134 (2004) 262-276.
39 [235] S. Rodrigues, N. Munichandraiah, A. Shukla, J Power Sources, 87 (2000) 12-20.
40 [236] H. Blanke, O. Bohlen, S. Buller, R.W. De Doncker, B. Fricke, A. Hammouche, D. Linzen, M. Thele,
41 D.U. Sauer, Journal of power Sources, 144 (2005) 418-425.
42 [237] A. Zenati, P. Desprez, H. Razik, S. Rael, in: 2010 IEEE Vehicle Power and Propulsion Conference,
43 IEEE, 2010, pp. 1-6.
44 [238] J. Xu, C.C. Mi, B. Cao, J. Cao, Journal of power sources, 233 (2013) 277-284.
45 [239] S. Nejad, D.T. Gladwin, D.A. Stone, in: IECON 2014-40th Annual Conference of the IEEE
46 Industrial Electronics Society, IEEE, 2014, pp. 5660-5665.
47 [240] J.-H. Lee, W.-J. Choi, Journal of Power Electronics, 11 (2011) 237-243.
48 [241] L. Ran, W. Junfeng, W. Haiying, L. Gechen, in: 2010 5th IEEE Conference on Industrial
49 Electronics and Applications, IEEE, 2010, pp. 684-688.
50 [242] A. Cuadras, O. Kanoun, in: 2009 6th International Multi-Conference on Systems, Signals and
51 Devices, IEEE, 2009, pp. 1-5.
52 [243] T. Osaka, T. Momma, D. Mukoyama, H. Nara, J Power Sources, 205 (2012) 483-486.
53 [244] Y. Ma, X. Zhou, B. Li, H. Chen, IEEE/CAA Journal of Automatica Sinica, 3 (2016) 281-287.
54
55
56
57
58
59
60

- 1
2
3 [245] V. Pizarro-Carmona, M. Cortés-Carmona, R. Palma-Behnke, W. Calderón-Muñoz, M.E. Orchard,
4 P.A. Estévez, *Energies*, 12 (2019) 681.
5 [246] H. Mu, R. Xiong, H. Zheng, Y. Chang, Z. Chen, *Appl Energ*, 207 (2017) 384-393.
6 [247] N. Chen, P. Zhang, J. Dai, W. Gui, *IEEE Access*, 8 (2020) 26872-26884.
7 [248] A. Podias, A. Pfrang, F. Di Persio, A. Kriston, S. Bobba, F. Mathieux, M. Messagie, L. Boon-Brett,
8 *World Electric Vehicle Journal*, 9 (2018) 24.
9 [249] P. Cicconi, D. Landi, A. Morbidoni, M. Germani, in: 2012 IEEE International Energy Conference
10 and Exhibition (ENERGYCON), IEEE, 2012, pp. 985-990.
11 [250] E. Martinez-Laserna, I. Gandiaga, E. Sarasketa-Zabala, J. Badeda, D.-I. Stroe, M. Swierczynski, A.
12 Goikoetxea, *Renewable and Sustainable Energy Reviews*, 93 (2018) 701-718.
13 [251] Panasonic, in, Panasonic Newsroom 2019.
14 [252] A. Devices, in, Analog Devices Circuit Note, 2019.
15
16
17
18
19
20
21
22
23
24
25
26
27
28
29
30
31
32
33
34
35
36
37
38
39
40
41
42
43
44
45
46
47
48
49
50
51
52
53
54
55
56
57
58
59
60